Interplay between the Conformational Flexibility and Photoluminescent Properties of Mononuclear Pyridinophanecopper(I) Complexes

Interplay between conformational flexibility and photoluminescent properties of mononuclear pyridinophane copper(I) complexes

Pradnya H. Patil,† Georgy A. Filonenko,† Sébastien Lapointe,† Robert R. Fayzullin‡ and Julia R. Khusnutdinova*†

† Coordination Chemistry and Catalysis Unit, Okinawa Institute of Science and Technology Graduate University, 1919-1 Tancha, Onna-son, Kunigami-gun, Okinawa, 904-0495 Japan

‡ Arbuzov Institute of Organic and Physical Chemistry, FRC Kazan Scientific Center of RAS, Arbuzov Street, 8, Kazan 420088, Russian Federation

Corresponding author: Julia Khusnutdinova (juliak@oist.jp)

KEYWORDS: Copper(I) complexes; Macrocyclic ligand; Steric bulk; Conformational dynamics; Photoluminescence.

ABSTRACT:

Macrocyclic ligand conformational behavior in solution, solid-state structures and photophysical properties of Cu(I) cationic and neutral mononuclear complexes supported by tetradentate N,N'-dialkyl-2,11-diaza[3.3](2,6)-pyridinophane ligands ^{R}N4 (R = H, Me, ^{i}Bu, ^{sec}Bu, ^{neo}Pent, ^{i}Pr, Ts) were investigated in detail. Steric properties of the alkyl group at the axial amine in the ^{R}N4

ligand were found to strongly affect the conformational preferences and dynamic behavior in solution. Several types of conformational exchange processes were revealed by VT NMR and EXSY, including degenerative exchange in a pseudotetrahedral species as well as exchange between two isomers with different conformers of a tri- and tetra-coordinate ^{R}N4 ligand. These exchange processes are slower for the complexes containing bulky alkyl groups at the amine as compared to less sterically demanding analogs. A clear correlation is also observed between the steric bulk of the alkyl substituents and photoluminescent properties of the derived complexes, with less dynamic complexes bearing bulkier alkyl substituents exhibiting higher absolute photoluminescence quantum yield (PLQY) in solution and in the solid state: PLQY in solution increases in the order Me $< ^{neo}$Pent $< ^{i}$Bu $< ^{sec}$Bu $\approx ^{i}$Pr $< ^{t}$Bu. The electrochemical properties of the cationic complexes [(^{R}N4)Cu^{I}(MeCN)]X (X = BF$_4$, PF$_6$) were also dependent on the steric properties of the amine substituent.

INTRODUCTION

During the past decades, photoluminescent materials have been widely utilized in sensors, an electroluminescent display, and probes of biological systems.[1-17] Among these materials, d^6 and d^8 transition metal complexes such as Ir^{III}, Ru^{II}, Os^{II}, Re^{I} and Pt^{II} are extensively used because of their stability, tunability and high efficiencies.[18-29] Another important class of photoluminescent compounds contain d^{10} coinage metal such as Ag^{I}, Au^{I} and Cu^{I}.[30-36] Among these compounds, Cu^{I} complexes are of considerable interest due to their low price and availability as an alternative to more expensive precious metal-based photoluminescent materials.[32, 37-39] Over the last several decades, a great variety of Cu^{I} photoluminescent complexes have been developed that include copper clusters, halide-bridged complexes, mono- and polynuclear phosphine complexes, homo-

or heteroleptic species with di-imine-type ligands, as well as recently developed N-heterocyclic carbene and amide complexes.[40-52] A variety of strategies were developed to control the emissive properties of Cu^I complexes, mostly based on variation of the supporting ligand electronic properties[42, 53, 54] or, in some cases, controlling configurational changes using steric properties of the ligand. [45, 55, 56] However, one of the common problems that can limit practical application of Cu^I complexes is their lability in solution leading to dissociation of polynuclear species or, in case of heteroleptic mononuclear complexes, ligand dissociation and exchange.[53, 57-59]

We have recently reported a series of solution-stable, photoluminescent mononuclear Cu^I complexes supported by the tetradentate ligand, N,N'-dialkyl-2,11-diaza[3.3](2,6)-pyridinophane, ^{R}N4.[60] These N-donor ligands are synthetically easily accessible and allow for various structural modifications by varying the nature of the amine substituent, while the macrocycle coordination to a Cu center leads to the formation of well-defined mononuclear complexes.[61] In particular, complexes A and B (Scheme 1, a) were found to be emissive in the solid state with the absolute photoluminescence quantum yield (PLQY) reaching 0.78 for complex A, but only 0.08 for complex B. Moreover, complex A also shows emission in dichloromethane solution at 25 ℃, while complex B was not emissive.

Another notable feature of these complexes was the conformational flexibility of the macrocyclic ligand in solution[62, 63] leading to the formation of two isomeric complexes (Scheme 1, b). In particular, we have reported that the cationic complexes [(^{R}N4)Cu^I(MeCN)]$^+$ and the neutral complexes A and B exist as two isomers in solution, in which the ^{R}N4 ligand binds to the Cu center with three N-donors or with all four N-donors coordinating in a κ^3 or κ^4-fashion, respectively.[60] Comparison of solution behavior of A and B studied by NMR spectroscopy showed that the ^{t}Bu-substituted complex A exists only as a tetracoordinate species in solution

with a κ^3-bound ^{tBu}**N4** ligand, while complex **B** exists in an equilibrium between two isomers with κ^3- and κ^4-bound ligands in a 61:39 ratio, respectively, at -35 °C. We hypothesized that this is due to the difference in steric bulk of the alkyl substituents at the axial amine donor rather than their electronic properties. Moreover, the greater flexibility of complex **B** could contribute to the absence of emission in solution in contrast to the *tert*-butyl-substituted complex **A**. However, the effect of the ester functional group in complex **B** could not be completely excluded as the length of the ester-containing substituent is sufficiently long to allow "wrapping around" the metal center resulting in weak interaction of the metal with the ester functional group and "exciplex" quenching. [38, 51, 64, 65] Therefore, comparison over a more diverse range of ligands is required to elucidate the role of structural factors in determining photophysical properties of the derived complexes.

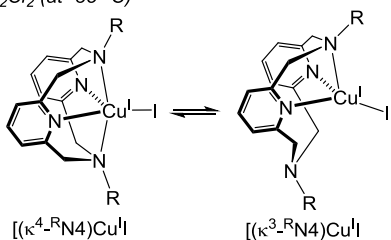**Scheme 1.** Previously reported (^{R}**N4**)Cu^{I}I complexes.[60]

a) Previously reported (^{R}N4)Cu^{I}I complexes and their photophysical properties (at 20 ^{o}C)
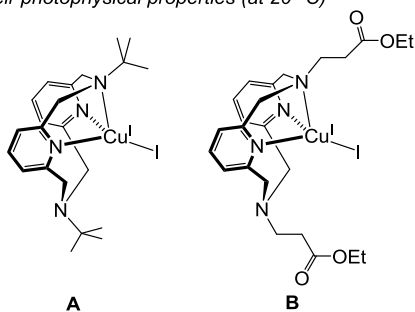
A
Φ (solid): 0.78
Φ (CH$_2$Cl$_2$ solution): 0.28

B
Φ (solid): 0.08
Φ (CH$_2$Cl$_2$ solution): N.D.

b) Conformational equilibria in solutions of **A** and **B** in CD$_2$Cl$_2$ (at -35 ^{o}C)

[(κ^4-^{R}N4)Cu^{I}I]   [(κ^3-^{R}N4)Cu^{I}I]

	κ^4	:	κ^3
A:	n.d		> 99
B:	39	:	61

We recently reported that ^{R}N4 ligand dynamic behavior in Cu^I complexes has an important implication in the development of mechanoresponsive polymer materials. We showed that the analogous ^{R}N4-based Cu^I complexes containing bulky alkyl group at the amine can be covalently attached to the polyurethane linear chain, acting as a stress-responsive photoluminescent probe showing fast and reversible emission intensity changes in response to tensile stress in polyurethane films.[66] Further studies showed that this is likely due to suppression of the non-radiative decay pathway in samples subjected to stress, likely reflecting dynamics within the macrocyclic ligand.[66]

In order to better design mechanoresponsive materials, we decided to carry out a systematic study into the main factors that affect the photophysical properties of complexes similar to the ones used in the Cu^I incorporated polyurethane study.

6

In the current work, we investigated in detail the solid-state structures, redox and photophysical properties, solution dynamic behavior and conformational equilibria in a series of cationic and neutral Cu^I complexes supported by the tetradentate pyridinophane-type ligands. We assessed the steric effect of the amine substituents on the conformational preference and dynamics in the series of cationic $[(^RN4)Cu^I(MeCN)]^+$ and neutral $(^RN4)Cu^II$ complexes where R = H, Me, ^iBu, ^{sec}Bu, $^{neo}Pent$, and ^iPr (Chart 1). In addition, the strength of the Cu^I interaction with axial amine donors was varied using electron-poor tosyl-substituted complexes $[(^{Ts}N4)Cu^I(MeCN)]^+$ and $(^{Ts}N4)Cu^II$ (Chart 1). The comparison of these complexes demonstrates that the steric properties of the amine substituent are the main factors controlling conformational preference and dynamic in solution as well as photophysical properties of the derived complexes. 2D Exchange Spectroscopy (EXSY) and variable temperature (VT) NMR spectroscopic studies also revealed several types of exchange processes involved in the conformational equilibria in solution. For both cationic and neutral complex series, increasing steric hindrance is associated with greater preference for the tetracoordinate complexes in solution. Moreover, steric hindrance was found to affect redox properties of the cationic complexes. The current study demonstrates that a synthetically simple modification of the axial amine steric properties leads to significant variation of emissive properties. This can be used as a strategy to design solution-stable mononuclear Cu^I complexes with macrocyclic N-donor ligands, by contrast to many other transition metal-based system where synthetically demanding variation of the electronic properties of the surrounding ligands is needed.
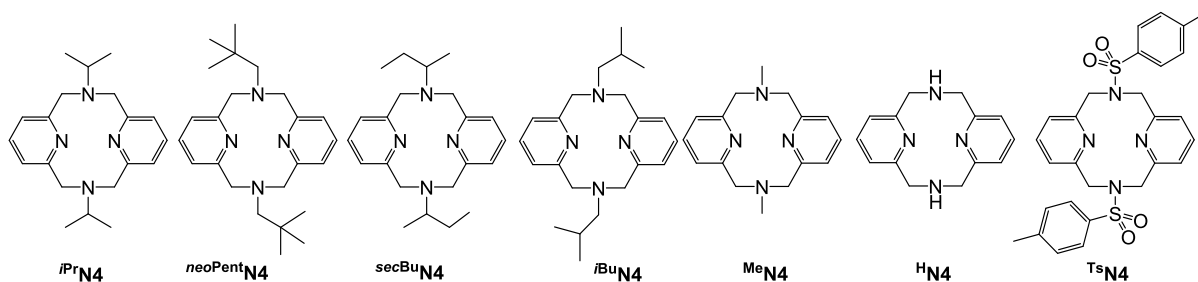
Chart 1. Ligands studied in this work.

EXPERIEMENTAL DETAILS

General specifications. All manipulations were carried out under an argon atmosphere using standard Schlenk and MBRAUN glove box techniques if not indicated otherwise. All reagents for which the synthesis is not given were commercially available from Sigma-Aldrich, TCI, Nacalai Tesque and were used as received without further purification. Anhydrous solvents were dispensed from an MBRAUN solvent purification system and degassed prior to use. Anhydrous deuterated solvents were purchased from Euriso-top and stored over 4Å molecular sieves.

Ligand N,N'-di-*iso*-propyl-2,11-diaza[3,3](2,6)pyridinophane ($^{i\text{Pr}}$N4), [67] N,N'-di-methyl-2,11-diaza[3,3](2,6)pyridinophane ($^{\text{Me}}$N4),[68] 2,11-diaza[3,3](2,6)pyridinophane ($^{\text{H}}$N4),[68] N,N'-di-tosyl-2,11-diaza[3,3](2,6)pyridinophane ($^{\text{Ts}}$N4),[68] were prepared according to the literature procedures. [Cu(MeCN)$_4$]$^+$ precursors were prepared by dissolving Cu$_2$O in acetonitrile solvent in the presence of aqueous HBF$_4$ or HPF$_6$ followed by two consecutive recrystallizations from cold acetonitrile.[69] NMR spectra were recorded on a JEOL ECZ400S 400MHz and ECZ600R 600MHz spectrometer. Chemical shifts are referenced internally to the residual solvent signals. 2D EXSY experiments were performed using NOESY pulse sequence; SST experiments were performed according to literature procedure.[70, 71] Full spectra and complete characterization data for all complexes are available in the Supporting Information. The signal abbreviation is as

follows: s, singlet; d, doublet; t, triplet; q, quartet; quin, quintet; sept, septet; m, multiplet; br, broad; Ar−H, aromatic proton; quaternary, quat. Elemental analyses were performed using an Exeter Analytical CE440 instrument. UV-vis spectra were recorded on an Agilent Cary 60 spectrophotometer and FT-IR spectra were recorded on a Cary 630 with ATR module. The photoluminescence measurements at varying concentrations were performed using a Hamamatsu Quantaurus-QY plus apparatus; the measurements at 298 K were performed in degassed dichloromethane solutions and at liquid nitrogen temperature in 2-methyl tetrahydrofuran. Photoluminescence lifetime was measured using the second harmonics of Spectra-Physics Mai Tai pulsed laser and a Hamamatsu Photonics Streak Scope camera. The decay data were fitted with a single exponential decay function unless specified otherwise. The quantum yield was measured using a Hamamatsu Photonics Quantaurus-QY system that established the variations in absolute QY to be within 5% for solid and solution samples (CH_2Cl_2, c = 1-5 μM) at 298 K and 77K. Cyclic voltammetry (CV) experiments were performed using ALS/CHI Electrochemical Analyzer 660E and 760E. Electrochemical grade $^nBu_4NPF_6$ and $^nBu_4NBF_4$ (Fluka) were used the supporting electrolyte. Electrochemical measurements were performed in an Ar-filled glove box. A Pt disk electrode (d = 1.6 mm) was used as the working electrode, and a Pt wire as the auxiliary electrode. The non-aqueous Ag-wire reference electrode assembly was filled with 0.01 M $AgNO_3$/0.1 M $^nBu_4NClO_4$/MeCN solution was used as a reference electrode and was calibrated against Cp_2Fe (Fc).

X-ray structure determination. The X-ray diffraction (XRD) data for the single crystals **1-10** were collected on a Rigaku XtaLab PRO instrument (ω-scan mode) with a PILATUS3 R 200K hybrid pixel array detector and a MicroMax[TM]-003 microfocus X-ray tube using Mo$K\alpha$ (0.71073 Å) radiation at low temperature. Images were indexed and integrated using the CrysAlis[Pro] data

reduction package. Data were corrected for systematic errors and absorption using the ABSPACK module: Numerical absorption correction based on Gaussian integration over a multifaceted crystal model and empirical absorption correction based on spherical harmonics according to the point group symmetry using equivalent reflections. The GRAL module and the ASSIGN SPACEGROUP routine of the WinGX suite[72] were used for analysis of systematic absences and space group determination. The structures were solved by the direct method using SHELXT[73] and refined by the full-matrix least-squares on F^2 using SHELXL.[74] Non-hydrogen atoms were refined anisotropically. The hydrogen atoms were inserted at the calculated positions and refined as riding atoms. The positions of the hydrogen atoms of methyl groups were found using rotating group refinement with idealized tetrahedral angles. Complex **6** crystallizes with two molecules A and B in the asymmetric cell ($Z' = 2$); complex **9** crystallizes with the molecule bisected by a mirror plane ($Z' = 0.5$). N4B-Pivot ^{neo}Pent (symmetrically independent molecule B) and N3-pivot ^{i}Bu substituents of **6** and **8**, respectively, are disordered into two positions. In the case of **7**, ^{sec}Bu fragment at atom N3 and N4- ^{sec}Bu moiety are involved in substitutional disordering with different configuration of chiral carbon atoms; the racemic composition of the whole unit cell is provided by crystallographic inversion symmetry. Interestingly, as a result of the mentioned disorder, non-coordinated nitrogen atom N4 shows either distorted pyramidal (N41) or almost planar (N42) configuration. The disorder was resolved using free variables and reasonable restraints on geometry and anisotropic displacement parameters. Achiral complexes **1** and **3** crystallize in the Sohncke space group $P2_12_12_1$ and the absolute structure of the crystals were determined by means of the Flack parameter.[75] All the compounds studied have no unusual bond lengths and angles. Section VI of the Supporting Information contains full experimental details regarding data collection and structure determination.

Synthesis of N,N'-di-*iso*-butyl-2,11-diaza[3,3](2,6)pyridinophane ($^{i\text{Bu}}$N4). (a) Synthesis of 2,6-bis-(*iso*-butylaminomethyl)pyridine: To a solution of 2,6-bis-bromomethyl pyridine (2.1 g, 7.8 mmol, 1 equiv.) in acetonitrile (10 mL) was added dropwise the solution of *iso*-butyl amine (5.74 g, 78.5 mmol, 10 equiv.) in acetonitrile (10 mL) over 25 minutes at room temperature. The mixture was stirred at room temperature for 17 hours. Acetonitrile was then removed on rotary evaporator and residual waxy oil was dissolved in dichloromethane and washed with concentrated aqueous potassium carbonate. The organic phase was collected, dried with sodium sulfate and concentrated to dryness. The resulting oil was distilled under vacuum at 65 °C (120 mTorr) to give diamine product that was used in the next step without additional purification. Yield: 1.23 g (63%). ^{1}H NMR (600 MHz, 25°C, CDCl$_3$): δ 7.58 (t, $^3J_{\text{HH}}$ = 7.6 Hz, *p-H*$_{\text{Py}}$, 1H), 7.16 (d, $^3J_{\text{HH}}$ = 7.7 Hz, *m-H*$_{\text{Py}}$, 2H), 3.88 (s, -Py-C*H$_2$*-NH-, 4H), 2.46 (d, $^3J_{\text{HH}}$ = 6.9 Hz, -NH-C*H$_2$*-CH-, 4H), 1.87 (s, N*H*-, 2H), 1.84-1.74 (m, -CH$_2$-C*H*-(CH$_3$)$_2$, 2H), 0.93 (d, $^3J_{\text{HH}}$ = 6.6 Hz, -CH-(C*H$_3$*)$_2$-, 12H). ^{13}C NMR (151 MHz, 25°C, CDCl$_3$): δ 159.7 (quat. *C*$_{\text{Py}}$), 136.9 (*p-C*$_{\text{Py}}$), 120.5 (*m-C*$_{\text{Py}}$), 57.9 (-NH-*C*H$_2$-CH), 55.6 (-Py-*C*H$_2$-NH-), 28.7 (-CH$_2$-*C*H-(CH$_3$)$_2$-), 20.9 (-CH-(*C*H$_3$)$_2$-).

(b) Synthesis of N,N'-di-*iso*-butyl-2,11-diaza[3,3](2,6)pyridinophane, ($^{i\text{Bu}}$N4): 2,6-bis-(*iso*-butylaminomethyl)pyridine (1.23 g, 4.93 mmol, 1.05 equiv.) was placed in a round bottom flask containing 20 mL benzene and 30 mL of 10% Na$_2$CO$_3$ aqueous solution. The mixture was heated to 80 °C and the solution of 2,6-bis-bromomethylpyridine (1.24 g, 4.69 mmol, 1 equiv.) was added dropwise to the hot reaction mixture over the period of 30 minutes. The reaction mixture was heated at 80 °C for 16 hours. After cooling to room temperature, the organic phase was collected using a separatory funnel. Evaporation of the solvent furnished white waxy solid containing the target compound. The crude was then extracted three times with 10 mL of

dichloromethane/hexane = 1/1 vol. mixture. The extracts were then evaporated to dryness to furnish the target macrocycle. Combined yield 1.03 g (58%). ^{1}H NMR (600 MHz, 25 °C, CDCl$_3$): δ 7.10 (t, $^3J_{HH}$ = 7.5 Hz, p-**H**$_{Py}$, 2H), 6.76 (d, $^3J_{HH}$ = 7.6 Hz, m-**H**$_{Py}$, 4H), 3.86 (s, -Py-C**H**$_2$-N-, 8H), 2.56 (d, $^3J_{HH}$ = 7.2 Hz, -N-C**H**$_2$-CH-, 4H), 1.98 (m, -CH$_2$-C**H**-(CH$_3$)$_2$, 2H), 1.08 (d, $^3J_{HH}$ = 6.6 Hz, -CH-(C**H**$_3$)$_2$-, 12H). ^{13}C NMR (151 MHz, 25 °C, CDCl$_3$): δ 158.4 (quat. **C**$_{Py}$), 135.5 (p-**C**$_{Py}$), 122.8 (m-**C**$_{Py}$), 69.0 (-N-**C**H$_2$-CH), 64.9 (-Py-**C**H$_2$-N-), 27.4 (-CH$_2$-**C**H-(CH$_3$)$_2$-), 21.1 (-CH-(**C**H$_3$)$_2$-). ESI-HRMS (m/z): calculated for [C$_{22}$H$_{32}$N$_4$·H$^+$:]: 353.2705; Found C$_{22}$H$_{32}$N$_4$·H$^+$: 353.2702.

Synthesis of N,N'-di-sec-butyl-2,11-diaza[3,3](2,6)pyridinophane, (^{secBu}N4): 2,11-diaza[3,3](2,6)pyridinophane (0.200 gm, 0.83 mmol, 1.0 equiv.), sec-butyl bromide (5.7 gm, 41.6 mmol, 50.0 equiv.; used as racemate), anhydrous K$_2$CO$_3$ (1.38 gm, 9.96 mmol, 12.0 equiv.) and dry MeCN (50 mL) were charged into 100 mL round-bottom flask with a magnetic stirring bar. The reaction mixture was refluxed under N$_2$ for 3 days. The solution was coOLED to RT and the solvent removed under reduced pressure. The residue was suspended in 50 mL of CH$_2$Cl$_2$ and then washed with 1M NaOH and water. The CH$_2$Cl$_2$ layer was isolated, dried over anhydrous K$_2$CO$_3$, evaporated and further dried under vacuum to give pale yellow powder. Yield: 208 mg (71%). ^{1}H NMR (400 MHz, 25 °C, CDCl$_3$): δ 7.08 (t, $^3J_{HH}$ = 7.7 Hz, p-**H**$_{Py}$, 2H), 6.74 (d, $^3J_{HH}$ = 7.7 Hz, m-**H**$_{Py}$, 4H), 3.96 (d, $^2J_{HH}$ = 12.2 Hz, Py-C**H**$_2$-N-, 4H), 3.81 (d, $^2J_{HH}$ = 12.2 Hz, Py-C**H**$_2$-N-, 4H), 2.95-2.87 (m, -N-C**H**-(CH$_3$)(CH$_2$CH$_3$), 2H), 1.83-1.72 (m, -CH-C**H**H-CH$_3$, 2H), 1.52-1.41 (m, -CH- CH**H**-CH$_3$, 2H), 1.19 (d, $^3J_{HH}$ = 6.4 Hz, N-CH-C**H**$_3$, 6H), 1.10 (t, $^3J_{HH}$ = 7.3 Hz, -CH$_2$-C**H**$_3$, 6H). ^{13}C NMR (100 MHz, 25 °C, CDCl$_3$): δ 159.3 (quat. **C**$_{Py}$), 135.8 (p-**C**$_{Py}$), 122.9 (m-**C**$_{Py}$), 65.70 (-N-**C**H-(CH$_3$)(CH$_2$CH$_3$)), 65.67 (-N-**C**H-(CH$_3$)(CH$_2$CH$_3$)-), 60.9 (br, Py-**C**H$_2$-N-), 28.1 (-CH-**C**H$_2$-CH$_3$-), 28.0 (-CH-**C**H$_2$-CH$_3$), 15.81 (-CH-**C**H$_3$), 15.76 (-CH-**C**H$_3$), 12.5

(-CH$_2$-CH$_3$); two sets of signals were observed in equal ratio for N-CH carbon atom of the *sec*-butyl group and adjacent carbons due to the presence of two diastereomers. ESI-HRMS (m/z): calculated for [C$_{22}$H$_{32}$N$_4$·H$^+$:]: 353.2700; Found C$_{22}$H$_{32}$N$_4$·H$^+$: 353.2700.

Synthesis of N,N'-di-*neo*-pentyl-2,11-diaza[3,3](2,6)pyridinophane (^neoPentN4). (a) Synthesis of 2,6-bis-(*neo*-pentylaminomethyl)pyridine: 2,6-Bis-bromomethyl pyridine (1.20 g, 4.53 mmol, 1.0 equiv.) was added slowly to the *neo*-pentyl amine (7.90 g, 90.6 mmol, 20.0 equiv.) at RT with stirring. The mixture was stirred at room temperature for 17 hours. Extra *neo*-pentyl amine was then removed on a rotary evaporator and the residual waxy oil was dissolved in dichloromethane and washed with concentrated aqueous potassium carbonate. The organic phase was collected, dried with sodium sulfate and concentrated to dryness. The resulting waxy solid was used in the next step without additional purification. Yield: 1.24 g (98%). ^{1}H NMR (600 MHz, 25 °C, CDCl$_3$): δ 7.61 (t, $^3J_{HH}$ = 7.6 Hz, *p-H*$_{Py}$, 1H), 7.21 (d, $^3J_{HH}$ = 7.7 Hz, *m-H*$_{Py}$, 2H), 3.96 (s, Py-C*H*$_2$-NH-, 4H), 2.84 (br s, 2H), 2.43 (s, -NH-C*H*$_2$-C-, 4H), 0.96 (s, -CH$_2$-C(C*H*$_3$)$_3$-, 18H). ^{13}C NMR (151 MHz, 25 °C, CDCl$_3$): δ 158.9 (quat. *C*$_{Py}$), 137.4 (*p-C*$_{Py}$), 120.9 (*m-C*$_{Py}$), 62.1 (Py-*C*H$_2$-NH-), 55.7 (-NH-*C*H$_2$-C-), 31.9 (-CH$_2$-*C*(CH$_3$)$_3$), 28.2 (-CH$_2$-C(*C*H$_3$)$_2$).

(b) Synthesis of N,N'-di-*neo*-pentyl-2,11-diaza[3,3](2,6)pyridinophane, (^neoPentN4): 2,6-bis-(*neo*-pentylaminomethyl)pyridine (1.24 g, 4.47 mmol, 1.0 equiv.) was placed in a round-bottom flask containing benzene (20 mL) and of 10% Na$_2$CO$_3$ (30 mL) aqueous solution. The mixture was heated to 80 °C and the solution of 2,6-bis-bromomethylpyridine (1.13 g, 4.25 mmol, 0.95 equiv.) was added dropwise to the hot reaction mixture over a period of 30 minutes. The reaction mixture was heated at 80 °C for 16 hours. After cooling to room temperature, the organic phase was collected using a separatory funnel. Evaporation of the solvent furnished a white, waxy solid containing the target compound. The crude was then treated with acetonitrile (15mL) and filtered

to remove insoluble white solid. The acetonitrile filtrate was extracted with hexane. The hexane layer was concentrated to give the target product as a white powder. Combined yield: 0.129 g (7 %) (combined yield). ^{1}H NMR (400 MHz, 25 °C, CDCl$_3$): δ 7.11 (t, $^3J_{HH}$ = 7.6 Hz, p-H_{Py}, 2H), 6.90 (d, $^3J_{HH}$ = 7.7 Hz, m-H_{Py}, 4H), 3.97 (s, -Py-CH_2-N-, 8H), 2.58 (s, -N-CH_2-C-, 4H), 1.09 (s, -C-(CH_3)$_3$, 18H). ^{13}C NMR (100 MHz, 25 °C, CDCl$_3$): δ 158.4 (quat. C_{Py}), 135.5 (p-C_{Py}), 122.8 (m-C_{Py}), 72.5 (-N-CH$_2$-C-), 67.7 (Py-CH$_2$-N-), 34.2 (-C(CH$_3$)$_3$), 28.1 (-C-(CH$_3$)$_3$-). ESI-HRMS (m/z): calculated for [C$_{24}$H$_{37}$N$_4$·H$^+$:]: 381.3013; Found C$_{24}$H$_{37}$N$_4$·H$^+$: 381.3010.

General procedure for the synthesis of [(^{R}N4)Cu^I(MeCN)]X (X = PF$_6$ or BF$_4$): To a stirred solution of the ligand (1.0 equiv.) in acetonitrile was added [Cu(MeCN)$_4$]PF$_6$ or [Cu(MeCN)$_4$]BF$_4$ (1.0 equiv.), which immediately produces red-orange solution. The reaction was stirred for 30 min, filtered through a celite plug, then recrystallized by slow diffusion of diethyl ether vapour over 1-2 days at room temperature. Crystalline solids were collected, washed with ether, hexane and dried under vacuum. Crystals suitable for X-ray analysis were obtained by diethyl ether vapor diffusion into acetonitrile solution of the complex. The details are given below for individual complexes and full characterization is given in the Supporting Information.

[(^{iPr}N4)Cu^I(MeCN)]PF$_6$ (1). Orange crystalline solid, isolated yield: 111 mg (63%). At -30 °C [(κ^4-^{iPr}N4)Cu^I(MeCN)]PF$_6$ and [(κ^3-^{iPr}N4)Cu^I(MeCN)]PF$_6$ isomers were present in CD$_3$CN solution 93.5:6.5 ratio by NMR integration. κ^4-**1**, major isomer: ^{1}H NMR (600 MHz, -30 °C, CD$_3$CN): δ 7.32 (t, $^3J_{HH}$ = 7.7 Hz, p-H_{Py}, 2H), 6.77 (d, $^3J_{HH}$ = 7.6 Hz, m-H_{Py}, 4H), 4.14 (d, $^2J_{HH}$ = 15.3 Hz, -Py-CH_2-N-, 4H), 3.60-3.53 (m, -N-CH-(CH$_3$)$_2$-, 2H), 3.54 (d, $^2J_{HH}$ = 15.3 Hz, -Py-CH_2-N-, 4H), 1.96 (s, CH_3CN, 3H), 1.31 (d, $^3J_{HH}$ = 6.6 Hz, -CH-(CH_3)$_2$-, 12H). ^{13}C NMR (151 MHz, -30 °C, CD$_3$CN): δ 157.2 (quat. C_{Py}), 137.3 (p-C_{Py}), 122.8 (m-C_{Py}), 58.0 (-CH-(CH$_3$)$_2$-),

57.7 (-Py-CH_2-N-), 18.9 (-CH-(CH_3)$_2$-). κ^3-**1**, minor isomer: ^{1}H NMR (600 MHz, -30 °C, CD$_3$CN): δ 7.40 (t, $^3J_{HH}$ = 7.7 Hz, p-H_{Py}, 2H), 6.99 (d, $^3J_{HH}$ = 7.7 Hz, m-H_{Py}, 2H), 6.82 (d, $^3J_{HH}$ = 7.7 Hz, m-H_{Py}, 2H), 4.29 (d, $^2J_{HH}$ = 15.2 Hz, -Py-CH_2-N-, 2H), 4.22 (d, $^2J_{HH}$ = 12.4 Hz, -Py-CH_2-N-, 2H), 4.02 (d, $^2J_{HH}$ = 12.4 Hz, -Py-CH_2-N-, 2H), 3.74 (d, $^2J_{HH}$ = 15.2 Hz, -Py-CH_2-N-, 2H), 1.39 (d, $^3J_{HH}$ = 6.5 Hz, -CH-(CH_3)$_2$-, 6H), 1.22 (d, $^3J_{HH}$ = 6.6 Hz, -CH-(CH_3)$_2$-, 6H). -CH-(CH$_3$)$_2$- peaks could not be observed because of its low intensity. ^{13}C NMR (151 MHz, -30 °C, CD$_3$CN): δ 159.2 (quat. C_{Py}), 155.3 (quat. C_{Py}), 138.3 (p-C_{Py}), 124.9 (m-C_{Py}), 122.4 (m-C_{Py}), 62.5 (-Py-CH$_2$-N- or -CH-(CH$_3$)$_2$-), 60.2 (-CH-(CH$_3$)$_2$- or -Py-CH$_2$-N-), 59.6 (-Py-CH$_2$-N- or -CH-(CH$_3$)$_2$-), 19.0 (-CH-(CH_3)$_2$-), 18. 7 (-CH-(CH_3)$_2$-). Anal. Found (calcd for C$_{22}$H$_{31}$CuF$_6$N$_5$P): C 45.68 (46.03), H 5.30 (5.44), N 11.99 (12.20).

[(^{Me}N4)Cu^I(MeCN)]BF$_4$ (2). Orange crystalline solid; isolated yield: 55 mg (65 %). At -26 °C, [(κ^4-^{Me}N4)Cu^I(MeCN)]BF$_4$ and [(κ^3-^{Me}N4)Cu^I(MeCN)]BF$_4$ isomers were present in CD$_3$CN solution 96.6:3.38 ratio by NMR integration. κ^4-**2**, major isomer: ^{1}H NMR (600 MHz, -26 °C, CD$_3$CN): δ 7.31 (t, $^3J_{HH}$ = 7.5 Hz, p-H_{Py}, 2H), 6.73 (d, $^3J_{HH}$ = 7.7 Hz, m-H_{Py}, 4H), 4.04 (d, $^2J_{HH}$ = 15.1 Hz, -Py-CH_2-N-, 4H), 3.54 (d, $^2J_{HH}$ = 15.1 Hz, -Py-CH_2-N-, 4H), 2.91 (s, -N-CH_3, 6H), 1.97 (s, CH_3CN, 3H). ^{13}C NMR (151 MHz, -26 °C, CD$_3$CN): δ 156.7 (quat. C_{Py}), 137.7 (p-C_{Py}), 122.8 (m-C_{Py}), 64.6 (-Py-CH$_2$-N-,), 49.0 (-N-CH$_3$). κ^3-**2**, minor conformer: ^{1}H NMR (600 MHz, -30 °C, CD$_3$CN): δ 7.45 (t, $^3J_{HH}$ = 7.5 Hz, p-H_{Py}, 2H), 7.00 (d, $^3J_{HH}$ = 7.9 Hz, m-H_{Py}, 2H), 6.89 (d, $^3J_{HH}$ = 7.3 Hz, m-H_{Py}, 2H), 4.34 (d, $^2J_{HH}$ = 13.5 Hz, -Py-CH_2-N-, 2H), 4.29 (d, $^2J_{HH}$ = 15.6 Hz, -Py-CH_2-N-, 2H), 4.19 (d, $^2J_{HH}$ = 13.5 Hz, -Py-CH_2-N-, 2H), 3.76 (d, $^2J_{HH}$ = 15.6 Hz, -Py-CH_2-N-, 2H), 3.03 (s, -N-CH_3, 6H). The ^{13}C peaks of [(κ^3-^{Me}N4)Cu^I(CH$_3$CN)]BF$_4$ could not be detected due to low intensity. Anal. Found (calcd for C$_{18}$H$_{23}$CuF$_4$N$_5$B): C 46.60 (47.02), H 4.93 (5.04), N 14.76 (15.23).

[(^{H}N4)Cu^I(MeCN)]PF$_6$ (3). Orange crystalline solid, isolated yield: 35 mg (17 %). At -30 $^\circ$C, [(κ^4-^{H}N4)Cu^I(MeCN)]PF$_6$ and [(κ^3-^{H}N4)Cu^I(MeCN)]PF$_6$ isomers were present in CD$_3$CN solution 87.3:12.7 ratio by NMR integration. κ^4-**3**, major isomer: ^{1}H NMR (600 MHz, -30 °C, CD$_3$CN): δ 7.33 (t, $^3J_{HH}$ = 7.7 Hz, *p*-**H**$_{Py}$, 2H), 6.81 (d, $^3J_{HH}$ = 7.7 Hz, *m*-**H**$_{Py}$, 4H), 4.27 (2 doublets, $^2J_{HH}$ = 15.9 Hz, -Py-C**H$_2$**-N-, 4H), 3.64 (d, $^2J_{HH}$ = 15.9 Hz, -Py-C**H$_2$**-N-, 4H), 3.60 (br. m, -CH$_2$-N**H**, 2H), 1.96 (s, C**H$_3$**CN, 3H). ^{13}C NMR (151 MHz, -30 °C, CD$_3$CN): δ 157.4 (quat. **C**$_{Py}$), 137.1 (*p*-**C**$_{Py}$), 122.6 (*m*-**C**$_{Py}$), 55.8 (-Py-**C**H$_2$-N-). κ^3-**3**, minor conformer: ^{1}H NMR (600 MHz, -30 °C, CD$_3$CN): δ 7.47 (t, $^3J_{HH}$ = 7.6 Hz, *p*-**H**$_{Py}$, 2H), 7.06 (d, $^3J_{HH}$ = 7.8 Hz, *m*-**H**$_{Py}$, 2H), 6.91 (d, $^3J_{HH}$ = 7.7 Hz, *m*-**H**$_{Py}$, 2H), 4.42 (d, $^2J_{HH}$ = 14.3 Hz, -Py-C**H$_2$**-N-, 2H), 4.41 (d, $^2J_{HH}$ = 16.1 Hz, -Py-C**H$_2$**-N-, 2H), 4.18 (d, $^2J_{HH}$ = 14.3 Hz, -Py-C**H$_2$**-N-, 2H), 3.80 (d, $^2J_{HH}$ = 16.1 Hz, -Py-C**H$_2$**-N-, 2H). ^{13}C NMR (151 MHz, -30 °C, CD$_3$CN): δ 155.7 (quat. **C**$_{Py}$), 138.8 (*p*-**C**$_{Py}$), 124.1 (*m*-**C**$_{Py}$), 122.4 (*m*-**C**$_{Py}$), 57.6 (-Py-**C**H$_2$-N-). Second inequivalent resonance of quat. **C**$_{Py}$ and –Py-**C**H$_2$-N group could not be detected in ^{13}C NMR due to overlap with other peaks and small intensity. Anal. Found (calcd for C$_{16}$H$_{19}$CuF$_6$N$_5$P): C 39.02 (39.23), H 3.71 (3.91), N 13.79 (14.30).

[(^{Ts}N4)Cu^I(MeCN)]PF$_6$ (4). Yellow crystalline solid, isolated yield: 29 mg (20 %, Low yield because product was sparingly soluble in acetonitrile). Complex **4** remains fluxional in CD$_3$CN solution even when coOLED down -30 $^\circ$C. The effective symmetry of the ligand is *C$_{2v}$*, which could be due to the presence of only the κ^4 isomer or due to a fast, unresolved exchange processes. ^{1}H NMR (600 MHz, -30 °C, CD$_3$CN): δ 7.89 (d, $^3J_{HH}$ = 7.8 Hz, -(SO$_2$)-C-C**H**-CH-$_{Ar}$, 4H), 7.66-7.42 (br. m, *p*-**H**$_{Py}$ and -C**H**-C-CH$_3$-$_{Ar}$, 6H), 7.08-6.83 (br. m, *m*-**H**$_{Py}$, 4H), 5.29 (br s, -Py-C**H$_2$**-N-, 4H), 3.59 (br s, -Py-C**H$_2$**-N-, 4H), 2.50 (s, C**H$_3$**-$_{Ar}$, 6H), 1.96 (s, C**H$_3$**CN, 3H). ^{13}C NMR (151 MHz, -30 °C, CD$_3$CN): δ 153.9 (quat. **C**$_{Py}$), 146.2 (-CH-**C**-CH$_3$-$_{Ar}$), 140.2 (-(SO$_2$)-**C**-

CH-$_{Ar}$), 138.9 (p-C_{Py}), 131.1 (CH-C-CH$_3$-$_{Ar}$), 129.1 (-(SO$_2$)-C-CH-CH-$_{Ar}$), 124.6 (m-C_{py}), 56.8 (-Py-CH$_2$-N-), 21.5 (CH$_3$-$_{Ar}$). Anal. Found (calcd for C$_{30}$H$_{31}$CuF$_6$N$_5$O$_4$PS$_2$): C 44.67 (45.14), H 3.88 (3.91), N 8.60 (8.77).

General procedure for the synthesis of (^{R}N4)Cu^{I}I (5-10): To a stirred solution of the ^{R}N4 (1.0 equiv.) in dry tetrahydrofuran was added CuI (0.95 equiv.) to immediately produce a bright yellow suspension. Within 10 minutes the suspended solids dissolved and after 2-5 h, bright yellow solid appeared. The tetrahydrofuran was removed by vacuum evaporation and dichloromethane (for ^{R}N4 complexes; R = Me, ^{i}Bu, ^{sec}Bu, ^{neo}Pent, ^{i}Pr) or dichloromethane-methanol solution (for ^{Ts}N4 complex) was added to dissolve all the reaction mixture. The solution was passed through a celite plug and allowed to crystallize by diethyl ether vapor diffusion over 1-2 days. Crystalline solids were collected, washed with ether, hexane and dried under vacuum. Crystals suitable for X-ray analysis were obtained by slow diffusion of diethyl ether vapors into dichloromethane (**5-9**) or dichloromethane-methanol (**10**) solution.

(^{iPr}N4)Cu^{I}I (5). Bright yellow crystalline solid, isolated yield: 120 mg (76 %). At -30 ^{o}C, [(κ^3-^{iPr}N4)Cu^{I}I] and [(κ^4-^{iPr}N4)Cu^{I}I] isomers were present in CD$_2$Cl$_2$ solution 91.2:8.8 ratio by NMR integration. κ^3-**5**, major isomer: ^{1}H NMR (600 MHz, -30 °C, CD$_2$Cl$_2$,): δ 7.27 (t, $^3J_{HH}$ = 7.7 Hz, p-H_{Py}, 2H), 6.89 (d, $^3J_{HH}$ = 7.8 Hz, m-H_{Py}, 2H), 6.68 (d, $^3J_{HH}$ = 7.8 Hz, m-H_{Py}, 2H), 4.85 (d, $^2J_{HH}$ = 12.9 Hz, -Py-CH$_2$-N-, 2H), 4.32 (d, $^2J_{HH}$ = 14.8 Hz, -Py-CH$_2$-N-, 2H), 3.94 (d, $^2J_{HH}$ = 12.9 Hz, -Py-CH$_2$-N-, 2H), 3.66-3.62 (m, -CH-(CH$_3$)$_2$-, 1H), 3.56 (d, $^2J_{HH}$ = 14.8 Hz, -Py-CH$_2$-N-, 2H), 3.26-3.21 (m, -CH-(CH$_3$)$_2$-, 1H), 1.46 (d, $^3J_{HH}$ = 6.7 Hz, -CH-(CH$_3$)$_2$, 6H), 1.23 (d, $^3J_{HH}$ = 6.7 Hz, -CH-(CH$_3$)$_2$, 6H). ^{13}C NMR (151 MHz, -30 °C, CD$_2$Cl$_2$): δ 159.8 (quat. C_{Py}), 154.6 (quat. C_{Py}), 136.7 (p-C_{Py}), 124.4 (m-C_{Py}), 121.4 (m-C_{Py}), 60.1 (-Py-CH$_2$-N-), 59.9 (-Py-CH$_2$-N-), 59.4 (-CH-(CH$_3$)$_2$-), 59.1 (-CH-(CH$_3$)$_2$-), 19.4 (-CH-(CH$_3$)$_2$), 19.2 (-CH-(CH$_3$)$_2$). κ^4-**5**, minor isomer: ^{1}H

NMR (600 MHz, -30 °C, CD$_2$Cl$_2$,): δ 7.22 (t, $^3J_{HH}$ =7.7 Hz, *p-**H**$_{Py}$*, 2H), 4.14 (d, $^2J_{HH}$ = 14.8 Hz, -Py-C**H**$_2$-N-, 4H), 3.74-3.70 (m, -C**H**-(CH$_3$)$_2$-, 2H), 3.42 (d, $^2J_{HH}$ = 14.8 Hz, -Py-C**H**$_2$-N-, 4H), 1.32 (br.d, -C**H**-(C**H**$_3$)$_2$, 12H). The peak of the *meta*-protons of pyridine cannot be detected due to their low intensity. ^{13}C NMR (151 MHz, -30 °C, CD$_2$Cl$_2$): δ 156.9 (quat. ***C**$_{Py}$*), 135.9 (*p-**C**$_{Py}$*), 121.9 (*m-**C**$_{Py}$*), 56.1 (-***C**H-(CH$_3$)$_2$-*). Py-***C**H_2-N-* and Methyl peaks might be merging with another isomer peaks. Anal. Found (calcd for (CH$_2$Cl$_2$).3C$_{20}$H$_{28}$CuIN$_4$): C 44.82 (44.96), H 5.17 (5.32), N 10.12 (10.31).

(**^{neoPent}N4)Cu^{I}I (6).** Bright orange crystalline solid, isolated yield: 99 mg (66 %). Complex **6** exists as a single isomer (κ^3-^{neoPent}N4)Cu^{I}I in CD$_2$Cl$_2$ solution at -30 °C. κ^3-**6**: ^{1}H NMR (600 MHz, -30 °C, CD$_2$Cl$_2$): δ 7.27 (t, $^3J_{HH}$ = 7.5 Hz, *p-**H**$_{Py}$*, 2H), 7.01 (d, $^3J_{HH}$ = 7.5 Hz, *m-**H**$_{Py}$*, 2H), 6.66 (d, $^3J_{HH}$ = 7.5 Hz, *m-**H**$_{Py}$*, 2H), 4.94 (d, $^2J_{HH}$ = 12.8 Hz, -Py-C**H**$_2$-N-, 2H), 4.45 (d, $^2J_{HH}$ = 14.9 Hz, -Py-C**H**$_2$-N-, 2H), 4.08 (d, $^2J_{HH}$ = 14.9 Hz, -Py-C**H**$_2$-N-, 2H), 4.01 (d, $^2J_{HH}$ = 12.8 Hz, -Py-C**H**$_2$-N, 2H), 3.48 (s, -N-C**H**$_2$-C(CH$_3$)-, 2H), 2.55 (s, -N-C**H**$_2$-C(CH$_3$)$_3$-, 2H), 1.12 (s, -C-(C**H**$_3$)$_3$, 9H), 0.99 (s, -C-(C**H**$_3$)$_3$, 9H). ^{13}C NMR (151 MHz, -30 °C, CD$_2$Cl$_2$): δ 158.4 (quat. ***C**$_{Py}$*), 155.5 (quat. ***C**$_{Py}$*), 136.7 (*p-**C**$_{Py}$*), 124.6 (*m-**C**$_{Py}$*), 121.7 (*m-**C**$_{Py}$*), 75.7 (-N-***C**H_2$-C-*), 71.2 (-N-***C**H_2$-C-*), 67.7 (-Py-***C**H_2$-N*), 63.7 (-Py-***C**H_2$-N*), 36.4 (-CH$_2$-***C**-(CH_3)_3*), 34.2 (-CH$_2$-***C**-(CH_3)_3*), 30.3 (-***C**-(**C**H_3)_3*), 27.7 (-***C**-(CH_3)_3*). Anal. Found (calcd for (C$_{22}$H$_{32}$N$_4$CuI): C 50.49 (50.48), H 6.22 (6.35), N 9.56 (9.81).

(**^{secBu}N4)Cu^{I}I (7).** Bright yellow crystalline solid, isolated yield: 64 mg (42%). Complex **7** exists as a single isomer (κ^3-^{secBu}N4)Cu^{I}I in CD$_2$Cl$_2$ solution at -30 °C. κ^3-**7**: ^{1}H NMR (600 MHz, -30 °C, CD$_2$Cl$_2$): δ 7.26 (t, $^3J_{HH}$ = 7.6 Hz, *p-**H**$_{Py}$*, 2H), 6.91 (d, $^3J_{HH}$ = 7.6 Hz, *m-**H**$_{Py}$*, 1H), 6.85 (d, $^3J_{HH}$ = 7.9 Hz, *m-**H**$_{Py}$*, 1H), 6.7-6.6 (m, two overlapping *m-**H**$_{Py}$*, 2H), 5.02 (dd, $^2J_{HH}$ = 2.4, 13.0 Hz, -Py-C**H**$_2$-N-, 1H), 4.76 (d, $^2J_{HH}$ = 13.0 Hz, -Py-C**H**$_2$-N-, 1H), 4.32-4.24 (m, two overlapping

C$\boldsymbol{H_2}$-N, 2H), 3.96-3.87 (m, two overlapping C$\boldsymbol{H_2}$-N, 2H), 3.60 (vd, $^2J_{HH}$ = 15.0 Hz, two overlapping C$\boldsymbol{H_2}$-N, 2H), 3.28-3.23 (m, -N-C$\boldsymbol{H}$-(CH$_3$)(CH$_2$CH$_3$), 1H), 2.91-2.85 (m, -N-C$\boldsymbol{H}$-(CH$_3$)(CH$_2$CH$_3$)-, 1H), 2.54-2.48 (m, -CH-C$\boldsymbol{H_2}$-CH$_3$, 1H), 1.74-1.67 (m, -CH-C$\boldsymbol{H_2}$-CH$_3$, 1H), 1.47-1.35 (m, -CH-C$\boldsymbol{H_2}$-CH$_3$, 2H), 1.42 (d, $^3J_{HH}$ = 6.7 Hz, -CH-C$\boldsymbol{H_3}$, 3H), 1.20 (d, $^3J_{HH}$ = 6.5 Hz, -CH-C$\boldsymbol{H_3}$-, 3H), 1.01 (t, $^3J_{HH}$ = 7.4 Hz, -CH$_2$-C$\boldsymbol{H_3}$, 3H), 1.00 (t, $^3J_{HH}$ = 7.3 Hz, -CH$_2$-C$\boldsymbol{H_3}$, 3H); four partially overlapping signals of *meta*-H of Py and eight signals for PyCH$_2$-arms are observed due to asymmetric environment caused by the presence of *sec*-butyl and κ^3-coordination of the ligand. ^{13}C NMR (151 MHz, -30 °C, CD$_2$Cl$_2$): δ 159.97, 159.92 and 159.88 (quat. $\boldsymbol{C}_{Py}$; two signals are not resolved due to overlap), 154.79, 154.70, 154.65 and 154.56 (quat. $\boldsymbol{C}_{Py}$), 136.69 (*p*-$\boldsymbol{C}_{Py}$), 124.60, 124.53, 124.46 and 124.39 (*m*-$\boldsymbol{C}_{Py}$), 121.57, 121.49, 121.41 and 121.33 (*m*-$\boldsymbol{C}_{Py}$), 66.39 and 65.52 (-N-$\boldsymbol{C}$H-CH$_3$), 62.94, 62.82, 60.89 (br), 59.53 (br), 58.25 and 58.12 (-Py-$\boldsymbol{C}$H$_2$-N), 27.63 and 27.62 (-$\boldsymbol{C}$H$_2$-CH$_3$), 15.83 and 15.61 (-CH-$\boldsymbol{C}$H$_3$), 11.87 (-CH$_2$-$\boldsymbol{C}$H$_3$); due to asymmetric environment caused by *sec*-butyl groups and the presence of two diastereomers, four sets of signals were observed for *meta*- and *para*-protons of Py and several overlapping sets of signals for aliphatic protons. Anal. Found (calcd for (C$_{22}$H$_{32}$N$_4$CuI): C 48.30 (48.67), H 5.80 (5.94), N 10.02 (10.32).

(**^{iBu}N4)Cu^{I}I (8).** Bright yellow crystalline solid, isolated yield: 78 mg (51 %). Complex **6** exists as a single isomer (κ^3-^{iBu}N4)Cu^{I}I in CD$_2$Cl$_2$ solution at -30 °C. κ^3-**8**: ^{1}H NMR (600 MHz, -30 °C, CD$_2$Cl$_2$): δ 7.30 (t, $^3J_{HH}$ = 7.6 Hz, *p*-$\boldsymbol{H}_{Py}$, 2H), 6.84 (d, $^3J_{HH}$ = 7.6 Hz, *m*-$\boldsymbol{H}_{Py}$, 2H), 6.73 (d, $^3J_{HH}$ = 7.5 Hz, *m*-$\boldsymbol{H}_{Py}$, 2H), 4.94 (d, $^2J_{HH}$ = 13.5 Hz, -Py-C$\boldsymbol{H_2}$-N-, 2H), 4.35 (d, $^2J_{HH}$ = 15.1 Hz, -Py-C$\boldsymbol{H_2}$-N-, 2H), 4.05 (d, $^2J_{HH}$ = 13.5 Hz, -Py-C$\boldsymbol{H_2}$-N-, 2H), 3.85 (d, $^2J_{HH}$ = 15.1 Hz, -Py-C$\boldsymbol{H_2}$-N-, 2H), 3.30 (d, $^3J_{HH}$ = 6.3 Hz, -N-C$\boldsymbol{H_2}$-CH-, 2H), 2.41 (d, $^3J_{HH}$ = 7.3 Hz, -N-C$\boldsymbol{H_2}$-CH-, 2H), 2.32-2.26 (m, -CH$_2$-C$\boldsymbol{H}$-(CH$_3$)$_2$, 1H), 2.01-1.95 (m, -CH$_2$-C$\boldsymbol{H}$-(CH$_3$)$_2$, 1H), 1.09 (d, $^3J_{HH}$ = 6.8

Hz, -CH-(CH_3)$_2$, 6H), 0.99 (d, $^3J_{HH}$ = 6.6 Hz, -CH-(CH_3)$_2$, 6H). ^{13}C NMR (151 MHz, -30 °C, CD$_2$Cl$_2$): δ 156.9 (quat. C_{Py}), 155.0 (quat. C_{Py}), 136.4 (p-C_{Py}), 124.0 (m-C_{Py}), 121.3 (m-C_{Py}), 71.3 (-N-CH$_2$-CH-), 63.7 (-N-CH$_2$-CH-) and (-Py-CH$_2$-C), 63.3 (-Py-CH$_2$-C), 26.9 (-CH$_2$-CH-(CH$_3$)$_2$), 26.1 (-CH$_2$-CH-(CH$_3$)$_2$), 22.8 (-CH-(CH$_3$)$_2$), 20.4 (-CH-(CH$_3$)$_2$). Anal. Found (calcd for (C$_{23}$H$_{34}$N$_4$CuI): C 48.72 (48.67), H 5.89 (5.94), N 10.35 (10.32).

(^{Me}N4)Cu^{I}I (9). Bright yellow crystalline solid, isolated yield: 101 mg (59 %). At -30 °C, [(κ^4-^{Me}N4)Cu^{I}I] and [(κ^3-^{Me}N4)Cu^{I}I] isomers were present in CD$_2$Cl$_2$ solution 63.5:36.5 ratio by NMR integration. κ^4-9, major isomer: ^{1}H NMR (600 MHz, -30 °C, CD$_2$Cl$_2$,): δ 7.20 (t, $^3J_{HH}$ = 7.9 Hz, p-H_{Py}, 2H), 6.61 (d, $^3J_{HH}$ = 7.4 Hz, m-H_{Py}, 4H), 4.03 (d, $^2J_{HH}$ = 14.8 Hz, -Py-CH_2-N-, 4H), 3.40 (d, $^2J_{HH}$ = 14.8 Hz, -Py-CH_2-N-, 4H), 2.90 (s, -N-CH_3, 6H). ^{13}C NMR (151 MHz, -30 °C, CD$_2$Cl$_2$): δ 156.2 (quat. C_{Py}), 136.0 (p-C_{Py}), 121.8 (m-C_{Py}), 64.5 (-Py-CH$_2$-N-), 50.1 (-N-CH$_3$). κ^3-7, minor conformer: δ 7.32 (t, $^3J_{HH}$ = 7.7 Hz, p-H_{Py}, 2H), 6.88 (d, $^3J_{HH}$ = 7.4 Hz, m-H_{Py}, 2H), 6.75 (d, $^3J_{HH}$ = 7.4 Hz, m-H_{Py}, 2H), 4.92 (d, $^2J_{HH}$ = 13.6 Hz, -Py-CH_2-N-, 2H), 4.29 (d, $^2J_{HH}$ = 15.3 Hz, -Py-CH_2-N-, 2H), 4.02 (d, $^2J_{HH}$ = 13.6 Hz, -Py-CH_2-N-, 2H), 3.62 (d, $^2J_{HH}$ = 15.3 Hz, -Py-CH_2-N-, 2H), 3.02 (s, -N-CH_3, 3H), 2.51 (s, -N-CH_3, 3H). ^{13}C NMR (151 MHz, -30 °C, CD$_2$Cl$_2$): δ 155.6 (quat. C_{Py}), 154.8 (quat. C_{Py}), 136.4 (p-C_{Py}), 124.1 (m-C_{Py}), 121.3 (m-C_{Py}), 66.2 (-Py-CH$_2$-N-), 64.9 (-Py-CH$_2$-N-), 50.7 (-N-CH$_3$), 43.9 (-N-CH$_3$). Anal. Found (calcd for (C$_{16}$H$_{20}$N$_4$CuI): C 41.77 (41.89), H 4.40 (4.39), N 11.88 (12.21).

(^{Ts}N4)Cu^{I}I (10). Bright yellow crystalline solid, isolated yield: 41 mg (30 %, low yield due to low solubility in dichloromethane). In CD$_2$Cl$_2$ complex 10 remains fluxional even at -80 °C. The effective symmetry of the ligand is C_{2v}, which could be due to either the presence of only one isomer, (κ^4-^{Ts}N4)Cu^{I}I or (κ^2-^{Ts}N4)Cu^{I}I, or due to unresolved fast exchange. Single isomer: ^{1}H NMR (600 MHz, -80 °C, CD$_2$Cl$_2$,): δ 7.71 (d, $^3J_{HH}$ = 7.7 Hz, -(SO$_2$)-C-CH-CH-$_{Ar}$, 4H), 7.38 (d,

$^3J_{HH}$ = 7.7 Hz, -CH-C-CH$_3$-$_{Ar}$, 4H), 7.32 (t, $^3J_{HH}$ = 7.3 Hz, p-H_{Py}, 2H), 7.06 (br. s, m-H_{Py}, 4H), 5.01 (br d, $^2J_{HH}$ = 11.2 Hz, -Py-CH_2-N-, 4H), 3.60 (br d, $^2J_{HH}$ = 11.2 Hz, -Py-CH_2-N-, 4H), 2.41 (s, CH_3-$_{Ar}$, 6H). ^{13}C NMR (151 MHz, -80 °C, CD$_2$Cl$_2$): δ 154.2 (quat. C_{Py}), 143.8 (CH-C-CH$_3$-$_{Ar}$), 137.0 (p-C_{Py}), 134.2 (-(SO$_2$)-C-CH-$_{Ar}$), 129.7 (-CH-C-CH$_3$-$_{Ar}$), 126.5 (-(SO$_2$)-C-CH-CH$_3$-$_{Ar}$), 122.8 (m-C_{Py}), 56.0 (-Py-CH$_2$-N-), 21.2 (CH$_3$-$_{Ar}$). Anal. Found (calcd for (CH$_2$Cl$_2$.C$_{28}$H$_{28}$CuIN$_4$O$_4$S$_2$): C 42.17 (42.27), H 3.65 (3.67), N 6.53 (6.80).

RESULTS AND DISCUSSION

Synthesis and solid-state structures.

a) Cationic complexes. Cationic Cu^I complexes with a series of pyridinophane ligands were synthesized by reacting [Cu(MeCN)$_4$]X (X = PF$_6$, BF$_4$) with 1 equiv. of the pyridinophane ligand (Scheme 2); they were isolated in an analytically pure form as orange (**1-3**) or yellow (**4**) crystalline solids in 17-66% yields. All these complexes were completely soluble in polar solvents such as CH$_3$CN, acetone and poorly soluble in non-polar solvents. All [(^{R}N4)Cu^I(MeCN)]PF$_6$/BF$_4$ (**1-4**) complexes reacted slowly with chlorinated solvents, CH$_2$Cl$_2$ and CHCl$_3$, to form the respective (^{R}N4)Cu^{I}Cl complexes. All cationic complexes were highly unstable in the presence of air both in solution and in the solid state. All obtained complexes were characterized by elemental analysis, NMR, UV-vis and FT-IR spectroscopy, and their solid-state structures were determined by single crystal XRD (Figure 1). Although complex of **2** with a PF$_6^-$ counter ion did not yield crystals suitable for X-ray analysis, the analogous complex **2** with BF$_4^-$ as a counter ion was analyzed by XRD. The attempted preparation of the cationic complex with ^{iBu}N4 failed to give the desired product in an analytically pure form under the same conditions even after multiple recrystallizations.

Scheme 2. Synthesis of cationic Cu[I] complexes.

1 (R = [i]Pr; X = PF$_6$)
2 (R = Me; X = BF$_4$)
3 (R = H; X = PF$_6$)
4 (R = Ts; X = PF$_6$)
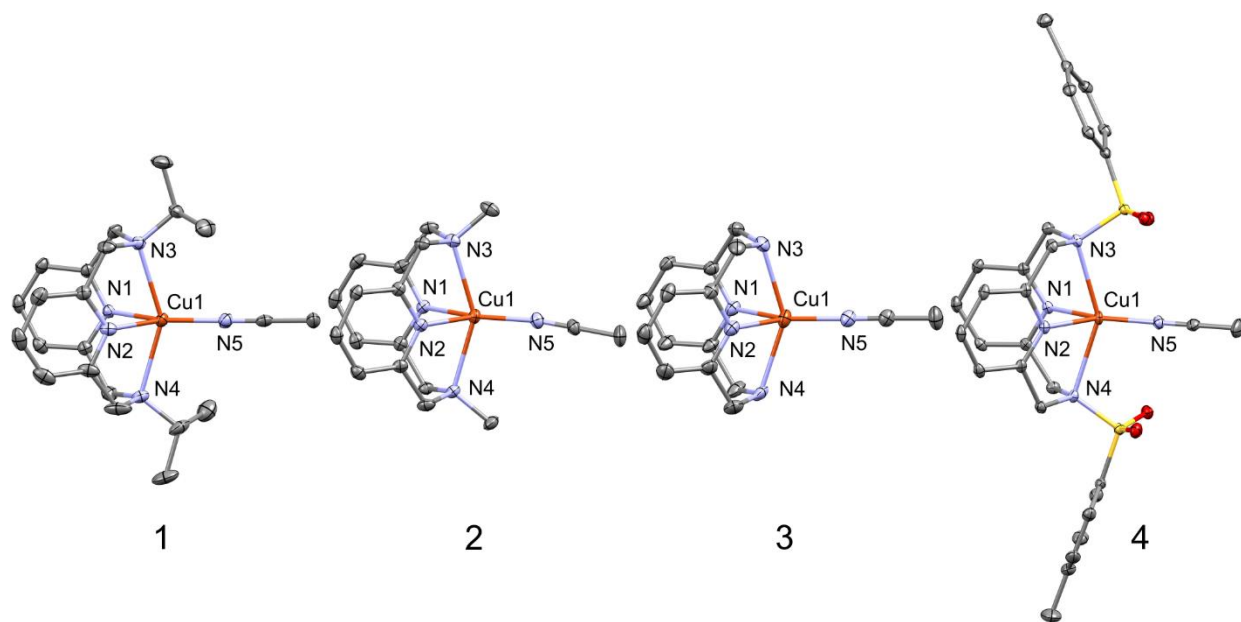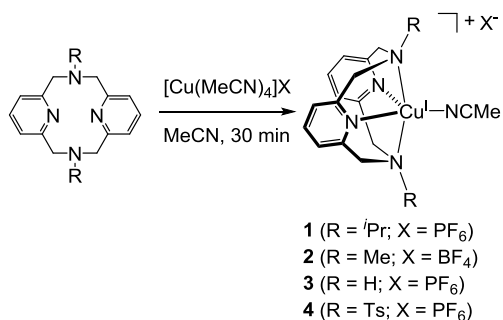
Figure 1. ORTEP projections of acetonitrile complexes **1-4** showing anisotropic displacement ellipsoids at 50 % probability level. Hydrogen atoms and counter ions are omitted for clarity.

The X-ray analysis reveals that the pyridinophane ligand **[R]N4** adopts a *syn*-boat-boat conformation[62, 63] in cationic Cu[I] complexes, featuring stronger coordination of the two pyridine rings and one MeCN ligand, and weaker interactions with the two axial amines. The coordination geometry of the Cu centers can be formally described as distorted square pyramidal[61] with τ_5 parameter values being closer to 0 expected from ideal square pyramidal geometry; however, the

22

Cu-N$_{amine}$ distances are significantly elongated compared to Cu-N$_{py}$ distances. The comparison

of bond distances in complexes $[(^{R}N4)Cu^{I}(MeCN)]^{+}$ **1-4** given in Table 1 shows that Cu-N$_{py}$ and

Cu-N$_{MeCN}$ bond distances are in a range of 1.88-2.10 Å typical for Cu^{I}-N bond lengths,[60, 61, 76-78,]

[79] while the Cu-N$_{amine}$ distances are significantly longer (Cu-N$_{amine}$ 2.35-2.49 Å). These structures

resemble those previously reported for other ^{R}N4-type pyridinophane Cu^{I} complexes.[60, 61] The

comparison of two analogous cationic complexes with different counter-anions,

$[(^{tBu}N4)Cu^{I}(MeCN)](PF_6)$ and $[(^{tBu}N4)Cu^{I}(MeCN)](BF_4)$, shows that bond distances and

coordination geometries are quite similar for both complexes.

Table 1. Selected Cu-N bond distances and τ_5 geometrical indices^{a} in complexes

$[(^{R}N4)Cu^{I}(MeCN)]X$ **1-4** and $[(^{tBu}N4)Cu^{I}(MeCN)]X$ (X =PF$_6$ or BF$_4$).

Complex	Cu1-N1, Å	Cu1-N2, Å	Cu1-N3, Å	Cu1-N4, Å	Cu1-N5, Å	τ_5^{a}
$[(^{tBu}N4)Cu^{I}(MeCN)](PF_6)^{b}$	2.089(2)	2.099(2)	2.444(2)	2.470(2)	1.901(2)	0.04
$[(^{tBu}N4)Cu^{I}(MeCN)](BF_4)^{b}$	2.0920(18)	2.0819(16)	2.4249(16)	2.4570(17)	1.8957(19)	0.08
$[(^{iPr}N4)Cu^{I}(MeCN)](PF_6)$ (**1**)	2.098(3)	2.082(3)	2.418(3)	2.400(3)	1.890(3)	0.14
$[(^{Me}N4)Cu^{I}(MeCN)](BF_4)$ (**2**)	2.0782(10)	2.0784(10)	2.3722(10)	2.3577(10)	1.8804(10)	0.03
$[(^{H}N4)Cu^{I}(MeCN)](PF_6)$ (**3**)	2.0892(15)	2.0937(16)	2.3510(17)	2.3653(17)	1.8824(16)	0.13
$[(^{Ts}N4)Cu^{I}(MeCN)](PF_6)$ (**4**)	2.0641(11)	2.0749(11)	2.4219(11)	2.4902(11)	1.8828(12)	0.15

^{a}The geometrical indices τ_5 for pentacoordinate structures are calculated according to Refs [80,81,82]; ^{b}From Ref [60]; atom numbering is corresponding to the one from Figure 1.

The comparison of Cu-N$_{amine}$ bond lengths (Cu1-N3 and Cu1-N4, Table 1) in complexes

$[(^{R}N4)Cu^{I}(MeCN)]X$ (**1-4**) as well as comparison with the published structures of

$[(^{tBu}N4)Cu^{I}(MeCN)]X$ with bulky ^{t}Bu groups at the amines reveals that greater steric hindrance

at the axial amine substituents leads to noticeable elongation of the Cu-N$_{amine}$ bond lengths in the

following order: R = ^{t}Bu > ^{i}Pr > Me > H. At the same time, complex **4** with a tosyl-substituted

amine features longest Cu-axial amine distances likely due to weak interactions with poorly donating N-Ts groups.

The ATR FT-IR spectra of polycrystalline samples of complexes [(^{iPr}N4)Cu^I(MeCN)]PF$_6$ (**1**), [(^{H}N4)Cu^I(MeCN)](PF$_6$) (**3**) and [(^{Ts}N4)Cu^I(MeCN)](PF$_6$) (**4**) are consistent with the presence of a non-coordinated PF$_6^-$ counter ion characterized by the 820-831 cm^{-1} band, while complex [(^{Me}N4)Cu^I(MeCN)](BF$_4$) (**2**) shows bands between 1047 and 1003 cm^{-1} that are typical for the BF$_4^-$ counter ion. The N-H stretching bands of the ^{H}N4 ligand appear at 3400 cm^{-1} for complex [(^{H}N4)Cu^I(MeCN)](PF$_6$) (**3**). For complex [(^{Ts}N4)Cu^I(MeCN)](PF$_6$) (**4**), the characteristic S=O and N-S stretching band appear at 1088 and 992 cm^{-1}, respectively.

b) Neutral copper(I) iodide complexes.

The neutral copper(I) iodide complexes were synthesized by mixing pyridinophane ligands with the anhydrous copper iodide in dry tetrahydrofuran to provide yellow (**5**, **7-10**) or orange (**6**) colored complexes (^{R}N4)Cu^{I}I (Scheme 3), which were isolated in an analytically pure form in 15-76% yields and characterized by elemental analysis, NMR and FT-IR spectroscopy. All these complexes were completely soluble in CH$_2$Cl$_2$ and acetone, and poorly soluble in non-polar solvents such as hexane, toluene, benzene and diethyl ether. These complexes show some limited stability in the crystalline state under air, but decompose in solution in the presence of oxygen. The ligand ^{H}N4 failed to give the desired product in a pure form under the same reaction conditions: a mixture of several complexes was obtained. Although the presence of the desired product (^{H}N4)Cu^{I}I was confirmed by XRD, it could not be separated from undesired by-products and could not be fully characterized.[83]

Scheme 3. Synthesis of neutral copper(I) iodide complexes.
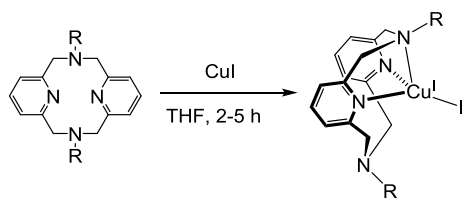
R = ^{i}Pr: ^{iPr}**N4**
R = ^{neo}Pent: ^{neopent}**N4**
R = ^{sec}Bu: ^{secBu}**N4**
R = ^{i}Bu: ^{iBu}**N4**
R = Me: ^{Me}**N4**
R = Ts: ^{Ts}**N4**

5 (R = ^{i}Pr)
6 (R = ^{neo}Pent)
7 (R = ^{sec}Bu)
8 (R = ^{i}Bu)
9 (R = Me)
10 (R = Ts)
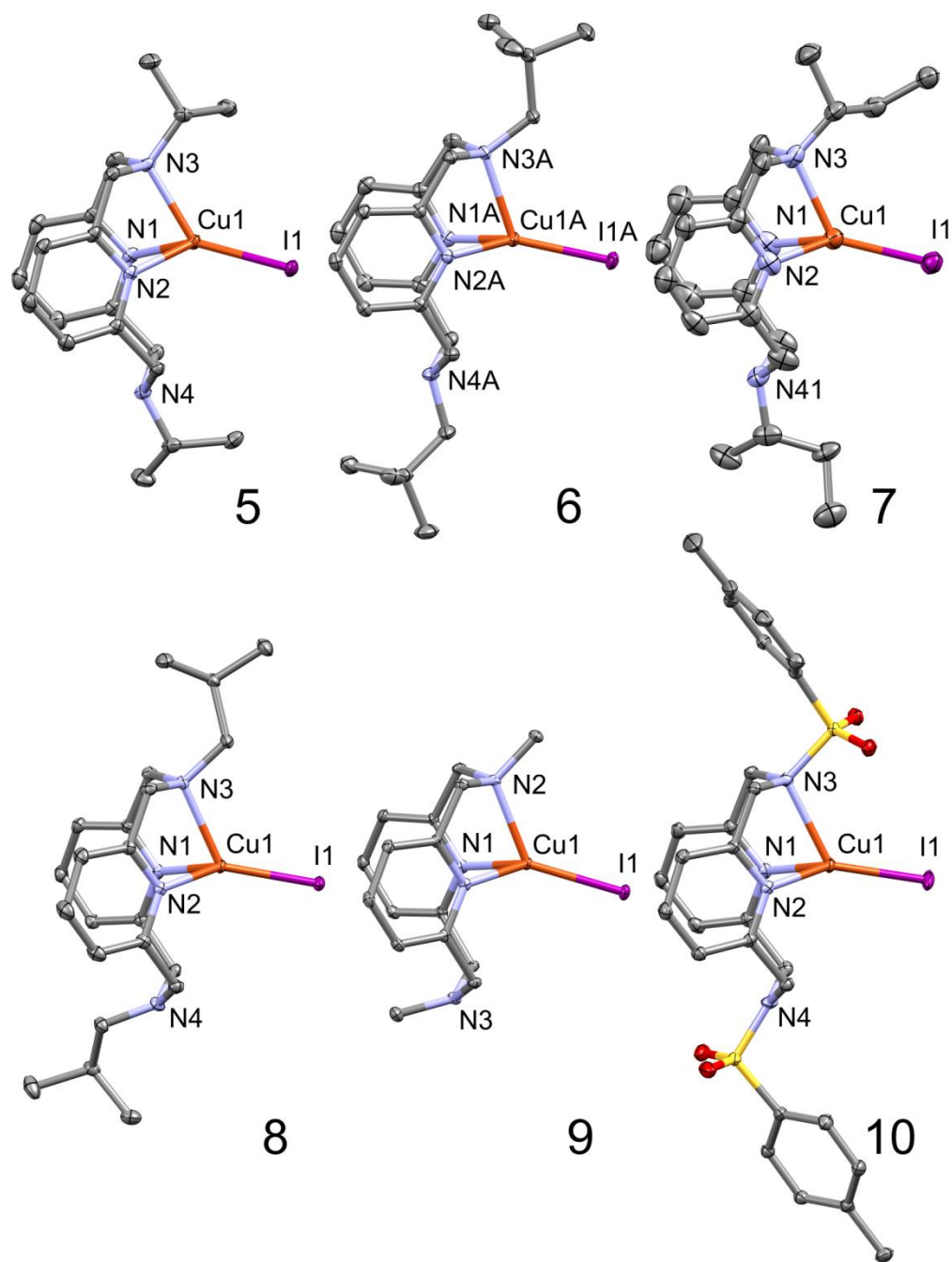
Figure 2. ORTEP projections of iodide complexes (^{R}N4)Cu^{I}I **5-10** showing anisotropic displacement ellipsoids at 50% probability level if not indicated otherwise. For complex **6**, only one independent molecule A is shown. For complex **7**, displacement ellipsoids are shown at 30% probability level for clarity. Hydrogen atoms, minor components of disorder and a solvent molecule in the case of (^{Ts}N4)Cu^{I}I **10** are omitted for clarity.

The X-ray crystal structures of complexes (^{R}N4)Cu^{I}I (**5-10**) display distorted tetrahedral coordination geometry around the Cu^I center with the pyridinophane ligand binding in a κ^3-fashion (Figure 2). The τ_4 and $\tau_{4'}$ parameters for tetracoordinate Cu centers in these complexes are in the range 0.53-0.68, indicative of noticeable deviation from ideal tetrahedral geometry where τ_4 and $\tau_4{'}$ equal to 1 are expected. In all complexes, the pyridinophane ligand adopts a *syn*-boat-chair conformation. These structures also resemble the previously reported tetracoordinate (^{tBu}N4)Cu^{I}I complex **A** (Scheme 1, a).[60] The selected bond lengths for complexes **5-8** and a previously reported tetracoordinate complex (^{tBu}N4)Cu^{I}I with ^{t}Bu-substituted pyridinophane ligand are summarized in Table 2. The Cu-axial amine distances in the solid state vary from 2.065 to 2.155 Å; however, no clear correlation with the steric properties of the alkylamine is observed, which could reflect the effect of crystal packing and intermolecular interactions, especially in the complexes where remote steric hindrance is present, (^{iBu}N4)Cu^{I}I and (^{neoPent}N4)Cu^{I}I. It should be noted that ^{sec}Bu and ^{i}Bu fragments at atom N3 for complexes (^{secBu}N4)Cu^{I}I (**7**) and (^{iBu}N4)Cu^{I}I (**8**) are disordered into two positions. Similar to complexes with alkyl-substituted ligands, (^{Ts}N4)Cu^{I}I (**10**) features a much longer Cu-axial amine bond owing to weak coordination of the tosylamide nitrogen.

Table 2. Selected Cu-N and Cu-I bond distances and geometrical indices^a (τ_4 and $\tau_4{'}$) in complexes (^{R}N4)Cu^{I}I **5-10** and (^{tBu}N4)Cu^{I}I **A**.

Complex	Cu1-N1, Å	Cu1-N2, Å	Cu1-N3, Å	Cu1-I1, Å	τ_4 and $\tau_{4'}$ values^a	
					τ_4	$\tau_{4'}$
(^{tBu}N4)Cu^{I}I (**A**)^b	2.1292(16)	2.1518(15)	2.2158(16)	2.4907(3)	0.67	0.66
(^{iPr}N4)Cu^{I}I (**5**)	2.1554(16)	2.1118(15)	2.2068(15)	2.4881(2)	0.62	0.60
(^{neoPent}N4)Cu^{I}I (**6A**)^c	2.1163(12)	2.1025(12)	2.2404(12)	2.46511(19)	0.63	0.62

|					
(^{neoPent}N4)Cu^{I}I (**6B**)^c	2.1136(12)	2.0688(12)	2.2560(12)	2.46202(19)	0.62	0.53
(^{secBu}N4)Cu^{I}I (**7**)	2.120(5)	2.117(5)	2.234(5)	2.4737(8)	0.66	0.62
(^{iBu}N4)Cu^{I}I (**8**)	2.0658(10)	2.0555(10)	2.2487(11)	2.46123(18)	0.68	0.64
(^{Me}N4)Cu^{I}I (**9**)	2.0876(13)	2.1978(17)^d	-	2.4755(3)	0.68	0.68
(^{Ts}N4)Cu^{I}I (**10**)	2.0967(16)	2.0849(16)	2.3467(17)	2.4600(3)	0.65	0.61

^{a}The geometrical indices τ_4 and τ_4' for tetracoordinate structures are calculated according to Refs [80,81,82] ^{b}From Ref[60]; atom numbering corresponds to Figure 2. ^{c}There are two molecules present in the asymmetric part of the unit cell. ^{d}The distance is related to the Cu-N$_{amine}$ bond (see numbering in Fig. 2). Complex (^{Me}N4)Cu^{I}I (**9**) crystallizes with the molecule bisected by a mirror plane, hence the asymmetric cell contains half of a molecule.

Macrocyclic ligand conformational flexibility in solution and NMR studies.

a) Cationic complexes. The dynamic behavior of the complexes was investigated by variable temperature, solution NMR study. Complexes [(^{R}N4)Cu^I(MeCN)]X (X = PF$_6$ or BF$_4$) where R = ^{i}Pr (**1**), Me (**2**), H (**3**), all featured slightly broadened ^{1}H resonances at room temperature (RT) indicative of the effective C_{2v} symmetry in solution. However, when the temperature was lowered to -30 °C, two isomers could be distinguished in solution under slow exchange conditions with clearly resolved, sharp proton resonances, except for complex [(^{Ts}N4)Cu^I(MeCN)](PF$_6$) (**4**), which remains fluxional (*vide infra*). The major isomer was assigned as a C_{2v}-symmetric [(κ^4-^{R}N4)Cu^I(MeCN)]$^+$, in which the ^{R}N4 ligand adopts a *syn*-boat-boat conformation binding to the Cu center with both pyridine and both axial amine N-atoms. This is evident from the presence of only one pair of doublets of the CH$_2$ groups showing geminal coupling ($J \approx 15$ Hz), and only one aromatic doublet of the pyridine *meta*-proton H$_{meta}$ integrating as 2:1 relative to the triplet of the *para*-proton of the pyridine, H$_{para}$. The minor isomer was assigned as the complex [(κ^3-^{R}N4)Cu^I(MeCN)]$^+$, where the ligand coordinates only with three N-atoms of pyridinophane, while one of the axial amines remains free. Accordingly, the CH$_2$ groups feature two pairs of geminally coupled doublets, and two inequivalent pyridine

H$_{meta}$ resonances are observed, consistent with an effective C_s symmetry of the ligand in solution. The ratio of [(κ^4-^{R}N4)Cu^I(MeCN)]$^+$ to [(κ^3-^{R}N4)Cu^I(MeCN)]$^+$ at -30 °C is dependent on the axial amine substituent; however, in all cases the [(κ^4-^{R}N4)Cu^I(MeCN)]$^+$ isomer remains predominant (Scheme 4).

Scheme 4. Isomers of [(^{R}N4)Cu^I(MeCN)]$^+$ (R = ^{i}Pr, Me, H) present in MeCN solution at -30 °C.

R		κ^4-isomer : κ^3-isomer
^{i}Pr	**1**	93.5 : 6.5
Me	**2**	96.6 : 3.4
H	**3**	87.3 : 12.7
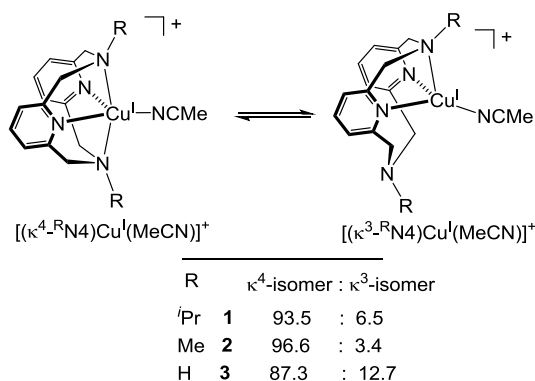
The complex [(^{Ts}N4)Cu^I(MeCN)](PF$_6$) (**4**) remains highly fluxional in solution even at -30 °C featuring broad, unresolved signals of methylene protons and pyridyl aromatic protons. This is consistent with fast configurational exchange due to the weak interactions of the copper center with poorly donating NTs axial donor groups that were observed in the solid state.

b) Neutral copper(I) iodide complexes. The solution behavior and exchange processes were studied in more detail for the series of copper iodide complexes (^{R}N4)Cu^{I}I (R = ^{t}Bu, ^{i}Pr, ^{neo}Pent, ^{sec}Bu, ^{i}Bu, Me) **5-10**. In contrast to the cationic complexes, the Cu^I iodide series displays photoluminescence not only in the solid state, but also in solution. The photoluminescence properties are likely strongly affected by the complexes' fluxional behavior (*vide infra*).

All above mentioned complexes (^{R}N4)Cu^{I}I (R = ^{t}Bu, ^{i}Pr, ^{neo}Pent, ^{sec}Bu, ^{i}Bu, Me) **5-10** are fluxional at RT featuring significantly broadened ligand resonances, which can be resolved upon cooling, with the coalescence temperature dependent on the substituent. The predominant isomer

for complexes (^{R}N4)Cu^{I}I (R = ^{t}Bu, ^{i}Pr, ^{neo}Pent, ^{sec}Bu, ^{i}Bu) in CD$_2$Cl$_2$ solution was a pseudotetrahedral complex (κ^3-^{R}N4)Cu^{I}I, in which the pyridinophane ligand binds only by three N-atoms, while one of the amine arms remains free. In the case of *iso*-propyl substituted complex **5**, the minor isomer, (κ^4-^{iPr}N4)Cu^{I}I, was also present in solution, with a (κ^4-^{iPr}N4)Cu^{I}I : (κ^3-^{iPr}N4)Cu^{I}I ratio of 8.8:91.2. By contrast, complex **9** with less sterically demanding methyl-substituted ligand ^{Me}N4 shows the opposite conformational preference, with (κ^4-^{Me}N4)Cu^{I}I complex being the predominant isomer (κ^4-^{Me}N4)Cu^{I}I : (κ^3-^{Me}N4)Cu^{I}I ratio of 63.5:36.5 (Scheme 5).

Scheme 5. Isomers of (κ^3-^{R}N4)Cu^{I}I present in CD$_2$Cl$_2$ solution (R = ^{t}Bu, ^{i}Pr, ^{neo}Pent, ^{sec}Bu, ^{i}Bu, Me) at -30 °C.

R:	κ^4	:	κ^3
^{t}Bu:	n.d		> 99
^{i}Pr:	8.8	:	91.2
^{neo}Pent:	n.d.		>99
^{sec}Bu:	n.d.		>99
^{i}Bu:	n.d.		>99
Me:	63.5	:	36.5
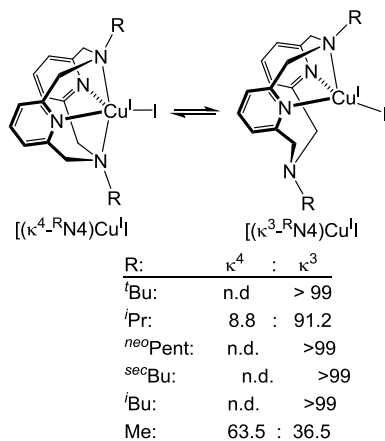
To further study the nature of processes involved in conformational exchange in complexes (^{R}N4)Cu^{I}I, 2D EXSY/NOESY NMR measurements were performed at low temperature under slow exchange conditions. Although the ^{1}H spectrum of **8**, (^{iBu}N4)Cu^{I}I, measured at -20 °C features only one conformer, (κ^3-^{iBu}N4)Cu^{I}I, the EXSY spectrum clearly reveals the exchange cross-peaks between two inequivalent resonances of pyridine *meta*-protons H$_m$ and H$_{m'}$ that appear in the same phase as the diagonal peaks (Figure 3). In addition, exchange cross-peaks are

also present between two pairs of the methylene doublets, H_a/H_b and $H_{a'}/H_{b'}$ that belong to CH_2 groups of the coordinated and non-coordinated axial amines (Figure 3). Accordingly, exchange cross-peaks are also seen between two sets of the corresponding multiplets of the *iso*-butyl groups. This is indicative of the degenerative mutual-site exchange process involving coordinated and free amine arms in complex $(\kappa^3\text{-}^{iBu}N4)Cu^I I$ as shown in Scheme 6. Upon warming, coalescence is observed between the resonances of H_m and $H_{m'}$, which merge into a single broad signal at *ca.* 23 °C (Figure 4).

Scheme 6. Exchange process in solution of $(\kappa^3\text{-}^R N4)Cu^I I$ (**5-10**) involving coordinated and non-coordinated amines (R = ^tBu, ^iPr, $^{neo}Pent$, ^{sec}Bu, ^iBu, Me).
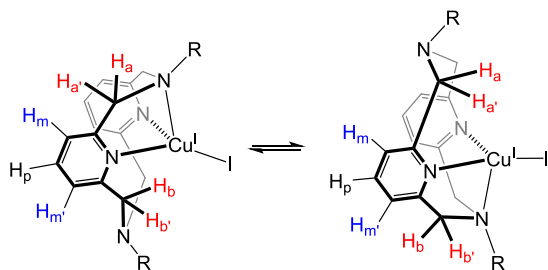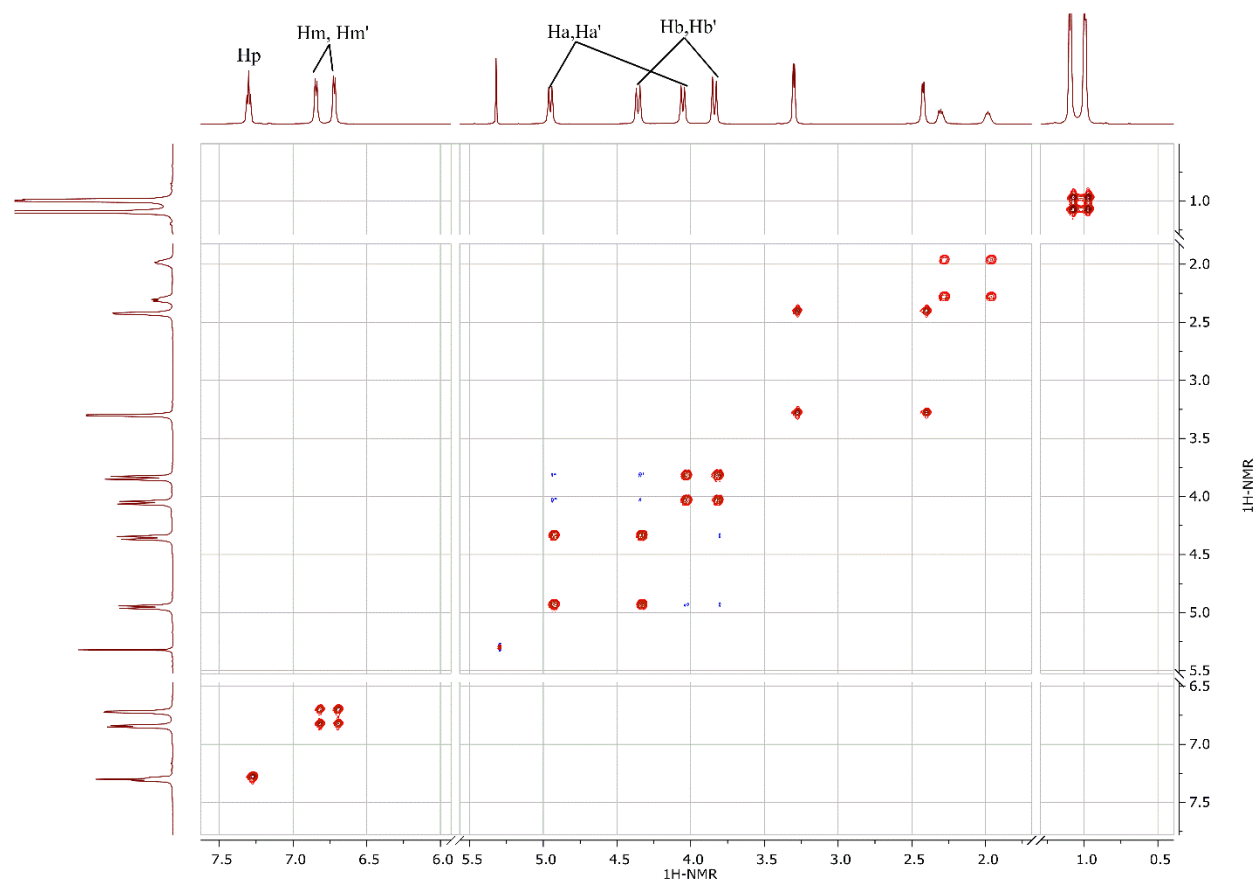
Figure 3. EXSY spectrum of complex (^{iBu}N4)Cu^{I}I (**8**) at -20 °C (mixing time 0.2 s). Exchange cross peaks are shown in red, in the same phase as the diagonal peaks (NOE cross-peaks are shown in blue, in the opposite phase to the diagonal peaks).
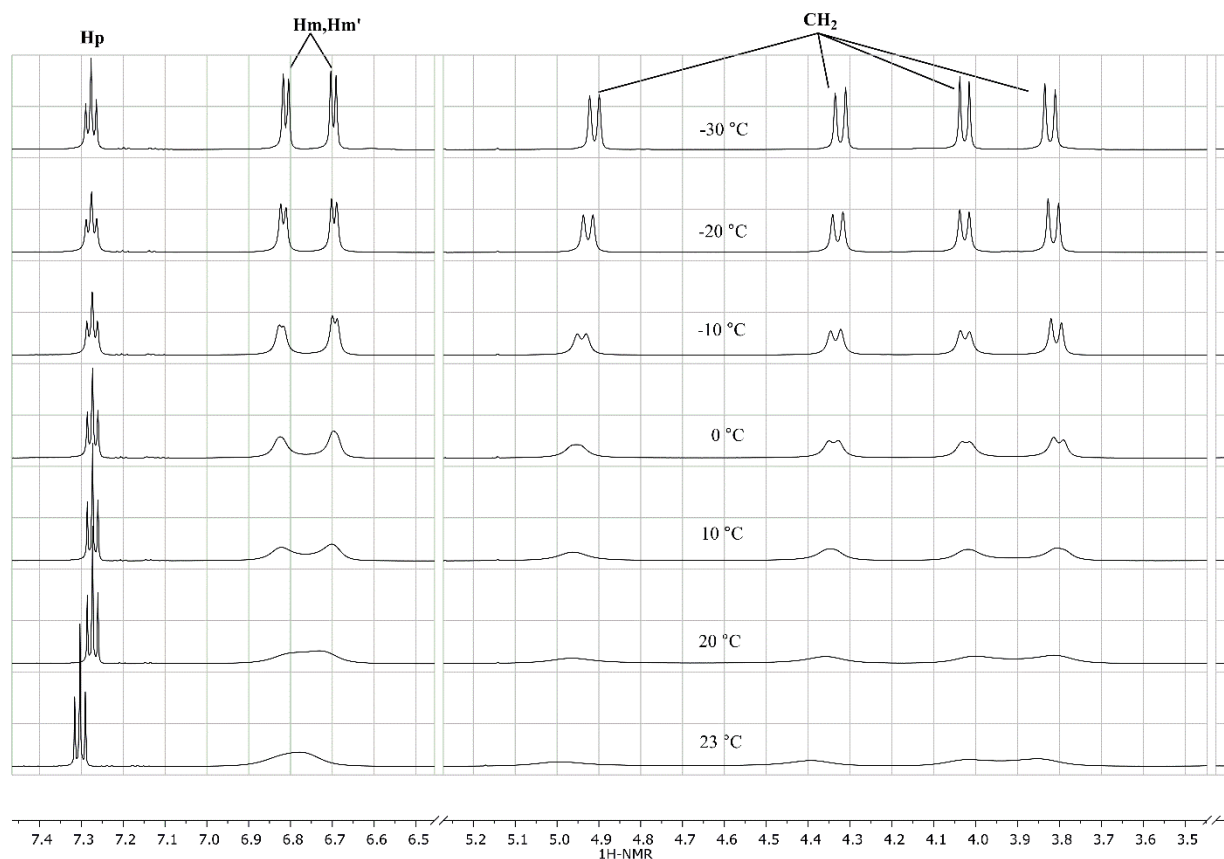
Figure 4. ^{1}H VT NMR spectra of complex (^{iBu}N4)Cu^{I}I (**8**) in CD$_2$Cl$_2$.

Similar exchange peaks were also observed by EXSY at -20 °C in complexes (^{tBu}N4)Cu^{I}I (**A**), (^{neoPent}N4)Cu^{I}I (**6**), (^{secBu}N4)Cu^{I}I (**7**) and for a major isomer of (^{iPr}N4)Cu^{I}I (**5**) containing a κ^3-bound ^{iPr}N4 ligand. However, the coalescence temperature for H$_m$ and H$_{m'}$ in these systems is higher when compared to the less bulky complex (^{iBu}N4)Cu^{I}I (**6**). Accordingly, in ^{i}Pr-substituted complex **5**, the coalescence temperature is *ca.* 35 °C, (^{neoPent}N4)Cu^{I}I, **6** showed the coalescence temperature at *ca.* 30 °C, at while in ^{t}Bu-substituted complex **A** and ^{sec}Bu-substituted complex **7**, the coalescence was not observed even at 35 °C. Since the chemical shift difference between H$_m$ and H$_{m'}$ remains similar (126 Hz) both for complexes (^{tBu}N4)Cu^{I}I (**A**) and (^{iPr}N4)Cu^{I}I (**5**),[84] this

indicates that complex **A** with a more bulky *t*Bu substituent is less fluxional in solution as compared to **5**.

This was further confirmed by variable temperature Spin Saturation Transfer (SST) NMR experiments in the case of complexes ($^{t\mathrm{Bu}}$N4)Cu$^{\mathrm{I}}$I (**A**), ($^{i\mathrm{Bu}}$N4)Cu$^{\mathrm{I}}$I (**8**) and ($^{neo\mathrm{Pent}}$N4)Cu$^{\mathrm{I}}$I (**6**) featuring a simple mutual-site exchange process.[85] The SST experiment was performed by irradiating one of the doublets of the *meta*-protons, which leads to the decrease in intensity of the signal of the second *meta*-proton, with the degree of suppression determined by the rate constant of exchange (Table 3, 4 and 5). The activation parameters are given in Table 6. The complex ($^{t\mathrm{Bu}}$N4)Cu$^{\mathrm{I}}$I (**A**) was the least fluxional among the series, while complexes featuring remote steric hindrance in *iso*-butyl and *neo*-pentyl groups, **8** and **6**, showed generally faster isomer exchange rates.

Table 3. Rate constant at various temperatures for $^{t\mathrm{Bu}}$N4Cu$^{\mathrm{I}}$I (complex **A**) in CD$_2$Cl$_2$.

Temperature (K)	Rate constant (k, s^{-1})
263	5.37
258	3.66
253	2.57
248	1.61
243	1.14
238	0.839
233	0.591

Table 4. Rate constants at various temperatures for $^{i\mathrm{Bu}}$N4Cu$^{\mathrm{I}}$I (complex **8**) in CD$_2$Cl$_2$.

Temperature (K)	Rate constant (k, s^{-1})
253	12.4

248	8.52
243	6.86
240.5	5.47
238	4.62
235.5	3.98
233	3.56
230.5	3.07

Table 5. Rate constants at various temperatures for $^{neo\text{Pent}}$N4Cu^{I}I (complex **6**) in CD$_2$Cl$_2$.

Temperature (K)	Rate constant (k, s-1)
255	7.15
253	5.88
251	4.73
249	4.06
247	3.26
243	2.07
241	1.74

Table 6. Activation parameters for complexes ($^{t\text{Bu}}$N4)Cu^{I}I **A**, ($^{i\text{Bu}}$N4)Cu^{I}I **8** and ($^{neo\text{Pent}}$N4)Cu^{I}I **6** determined from VT SST experiments.[a]

	($^{t\text{Bu}}$N4)Cu^{I}I (**A**)	($^{i\text{Bu}}$N4)Cu^{I}I (**8**)	($^{neo\text{Pent}}$N4)Cu^{I}I (**6**)
$\Delta H^{\neq}$(kcal·mol^{-1})	8.5±0.8	6.7±0.6	11.9±0.5
$\Delta S^{\neq}$(cal·mol^{-1}·K^{-1})	-23±3	-27±2	-7.4±2.1

$\Delta G^{\neq}$ (kcal·mol^{-1})^{b}	15.3±0.8	14.7±0.6	14.2±0.5
E_A (kcal·mol^{-1})^{c}	9.0±0.8	7.2±0.6	12.4±0.5
lnA^{d}	19±2	17±1	26±1

[a]All experiments were repeated three times at each temperature; see details in the Supp. Info. [b]As measurements could not be done at RT directly, $\Delta G^{\neq}$ was extrapolated to 298 K by using $\Delta H^{\neq}$ and $\Delta S^{\neq}$ values obtained above. [c]Arrhenius activation energy. [d]Natural logarithm of pre-exponential factor.

As discussed above, the complex (^{Me}N4)Cu^{I}I (**9**) features two isomers in solution, (κ^{4}-^{Me}N4)Cu^{I}I and (κ^{3}-^{Me}N4)Cu^{I}I, in comparable amounts, which allows for the observation of two types of exchange by EXSY NMR at -20 °C. First, similar to complexes (^{iPr}N4)Cu^{I}I (**5**), (^{iBu}N4)Cu^{I}I (**8**) and (^{tBu}N4)Cu^{I}I (**A**), the degenerative exchange between coordinated and non-coordinated amines is evident in (κ^{3}-^{Me}N4)Cu^{I}I isomer, with the coalescence between H_m and $H_{m'}$ observed at *ca.* 15 °C, showing that Me-substituted complex undergoes faster conformational exchange as compared to the bulkier ^{t}Bu, ^{i}Pr, ^{neo}Pent, ^{sec}Bu, and ^{i}Bu-substituted analogs **A** , **5**, **6**, **7** and **8**. The EXSY experiment also exhibits interconversion that occurs between the complexes with two different conformers of the ligand, (κ^{4}-^{Me}N4)Cu^{I}I and (κ^{3}-^{Me}N4)Cu^{I}I (Figure 5). For example, exchange cross peaks are observed between two *para*-protons of pyridines, H_p and $H_{p'}$, that belong to isomers (κ^{3}-^{Me}N4)Cu^{I}I and (κ^{4}-^{Me}N4)Cu^{I}I, respectively. Accordingly, both *meta*-protons of pyridines in (κ^{3}-^{Me}N4)Cu^{I}I, H_m and $H_{m'}$, exchange with the signal of $H_{m''}$ corresponding to pyridine *meta*-protons of the C_{2v}-symmetrical isomer (κ^{4}-^{Me}N4)Cu^{I}I (Scheme 7). Similarly, exchange-cross peaks are clearly seen between N-Me groups that belong to κ^{3}- and κ^{4}-isomers, Me$_a$, Me$_b$ and Me$_c$. Upon warming up, the resonances of N-Me of both isomers coalesce at *ca.* 21 °C (Figure 6).

Overall, qualitative comparison of solution behavior of complexes with alkylamine axial donors, (^{R}N4)Cu^{I}I indicates that the steric bulk of the alkyl group of the axial amines has a dual effect on the conformational behavior of the derived complexes: (*i*) increasing steric bulk of R substituent leads to higher preference towards the isomer with a κ^{3}-bound ^{R}N4 ligand; (*ii*) increasing steric bulk of the alkyl R groups slows down conformational exchange in these systems.

Scheme 7. Isomer interconversion involving (κ^{3}-^{Me}N4)Cu^{I}I and (κ^{4}-^{Me}N4)Cu^{I}I.
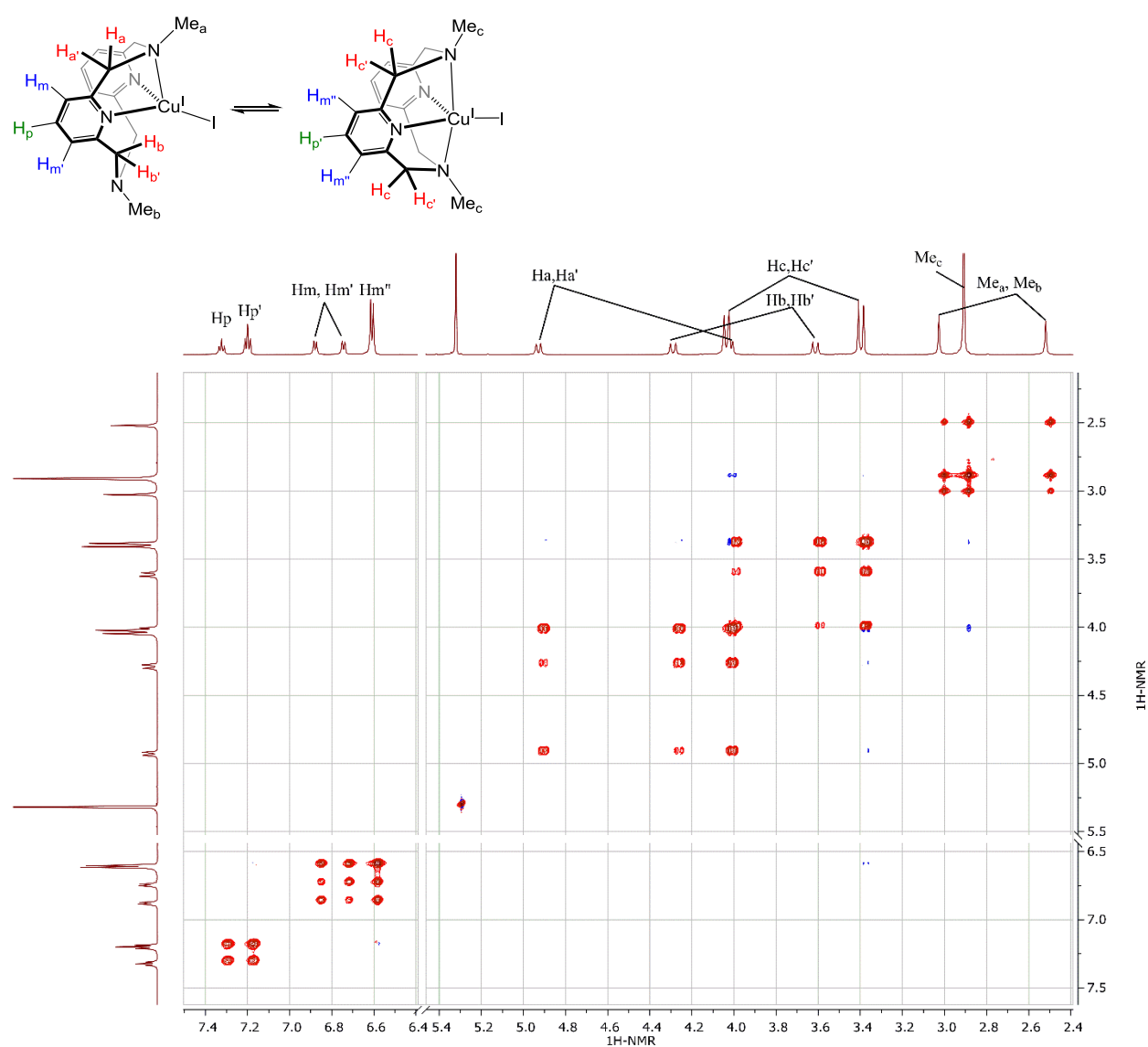
Figure 5. EXSY spectrum of complex (^{Me}N4)Cu^{I}I (**9**) at -20 °C (mixing time 0.2 s). Exchange cross peaks are shown in red, in the same phase as the diagonal peaks (NOE cross-peaks are shown in blue, in the opposite phase to the diagonal peaks).
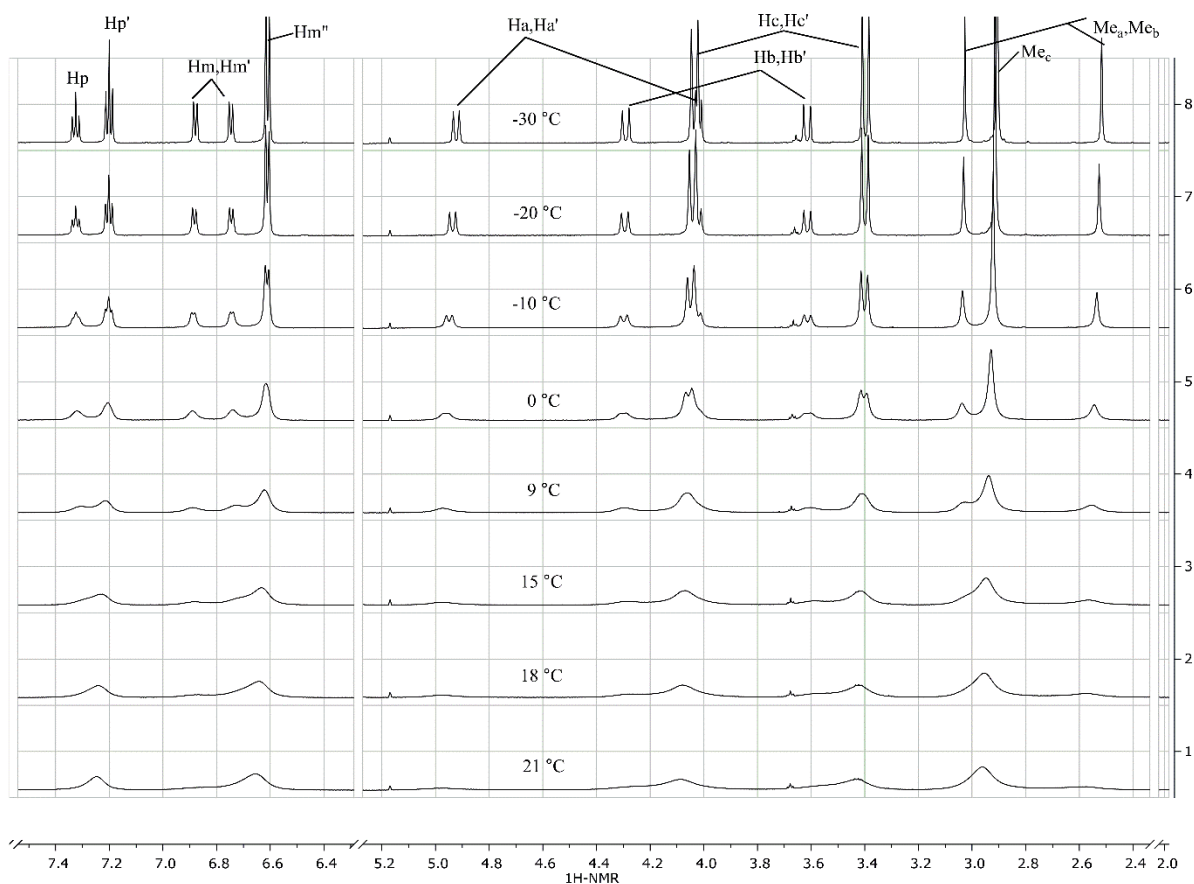
Figure 6. ^{1}H VT NMR spectra of complex (^{Me}N4)Cu^{I}I (**9**) in CD$_2$Cl$_2$.

As compared to the alkylamine analogs, the tosyl-substituted complex (^{Ts}N4)Cu^{I}I (**10**) undergoes much faster conformational exchange, so that slow exchange conditions could not be reached even at -80 °C. This is likely due to the weak coordination of the electron deficient N-Ts group to the Cu^I center, also consistent with significantly longer Cu^I-N bond distances observed in complex (^{Ts}N4)Cu^{I}I (**10**) when compared to the alkyl amine derivatives (even the ones with the bulky ^{t}Bu and ^{i}Pr groups). The ^{1}H NMR spectrum of (^{Ts}N4)Cu^{I}I at -80 °C features two

broadened doublets of CH_2 groups and only one signal corresponding to *meta*-protons of pyridines, indicative with the effective C_{2v} symmetry in solution. While this could be consistent with κ^4- (or κ^2-) coordination of the ^{Ts}N4 ligand in solution, high fluxionality of this complex does not allow unambiguous assignment of the conformational preference as the observed signals could also result from exchange between several configurational isomers leading to effective averaging of the signals.

Electrochemical properties. The electrochemical properties of cationic and neutral pyridinophane complexes were studied by cyclic voltammetry (Figure 7). The cationic complexes were examined by CV in MeCN solution using ^{n}Bu$_4$NPF$_6$ (for $[(^{iPr}N4)Cu^I(MeCN)]PF_6$ **1**, $[(^HN4)Cu^I(MeCN)]PF_6$ **3**, and $[(^{Ts}N4)Cu^I(MeCN)]PF_6$ **4**) and ^{n}Bu$_4$NBF$_4$ (for $[(^{Me}N4)Cu^I(MeCN)]BF_4$ **2**) as a supporting electrolyte: their electrochemical properties are summarized in Table 7. For all cationic complexes except Ts-substituted compound **4**, the chemically reversible oxidation wave assigned to a Cu^I/Cu^{II} oxidation event was observed. The separation between the forward and reverse peaks was in a range of 55-89 mV, larger than expected for an electrochemically reversible process for majority of complexes except the least sterically hindered $[(^HN4)Cu^I(MeCN)]PF_6$ (**3**).[86] This is likely due to significant structural changes that occur during oxidation of the pentacoordinate Cu^I center to form hexacoordinate Cu^{II} species. According to a literature example, a similar large separation between the anodic and cathodic peaks was observed in complex $[(^{tBu}N4)Cu^I(MeCN)]X$ (X = PF$_6$, OTf).[61] In this earlier work, the oxidation product, Cu^{II} complex $[(^{tBu}N4)Cu^{II}(MeCN)_2](OTf)_2$, was previously obtained and structurally characterized. Complex $[(^{tBu}N4)Cu^{II}(MeCN)_2](OTf)_2$ featured a distorted octahedral Cu^{II} center with two MeCN ligands

and with significantly shortened Cu-axial amine bond distances as compared to its Cu^I analog [$(^{tBu}N4)Cu^I(MeCN)$](OTf).[61]

Table 7. Electrochemical properties of complexes [$(^R N4)Cu^I(MeCN)$]X **1-4** (X = PF_6 or BF_4).[a]

Complex	E_{pf} (mV)[b]	E_{pr} (mV)[c]	ΔE (mV)[d]	$E_{1/2}$ (mV)[e]
[$(^{iPr}N4)Cu^I(MeCN)$](PF_6) (**1**)	-163	-249	89	-206
[$(^{Me}N4)Cu^I(MeCN)$](BF_4) (**2**)[f]	-241	-316	75	-279
[$(^H N4)Cu^I(MeCN)$](PF_6) (**3**)	-289	-344	55	-317
[$(^{Ts}N4)Cu^I(MeCN)$](PF_6) (**4**)[g]	674	-205	-	-

[a] Cyclic voltammograms for complexes for [$(^R N4)Cu^I(MeCN)$]X **1-4** (1 mM) in 0.1 M solution of $^n Bu_4 NPF_6$ (for **1**, **3**, **4**) or $^n Bu_4 NBF_4$ (for **2**) as a supporting electrolyte in acetonitrile at 23 °C, 100 mV/s scan rate, Pt disk electrode (*d* = 1.6 mm), all peaks were references vs. ferrocene. [b] Potential of the forward peak. [c] Potential of the return peak. [d] Peak-to-peak separation ΔE is calculated as $E_{pf} - E_{pr}$. [e] $E_{1/2}$ estimated as $1/2 \cdot (E_{pf} + E_{pr})$. [f] $^n Bu_4 NBF_4$ was used as an electrolyte. [g] Irreversible oxidation.

Interestingly, the estimated $E_{1/2}$ of Cu^I/Cu^{II} oxidation wave varies depending on the substituents at the amine axial donors, with the most positive $E_{1/2}$ being observed for the complex with the bulkiest ^iPr-substituent, [$(^{iPr}N4)Cu^I(MeCN)$]PF_6 (**1**), and most negative $E_{1/2}$ observed for the least sterically hindered complex [$(^H N4)Cu^I(MeCN)$]PF_6 (**3**). This trend is different to what could have been expected based solely on the donor properties of the axial amines, and it likely reflects the degree of stabilization of the Cu^{II} product due to differences in the steric bulk of the axial donor. Since significantly shorter $Cu-N_{amine}$ bond distances are expected for the oxidized Cu^{II} complex, more effective stabilization is expected from the least bulky ligands.

As compared to complexes **1-3**, the Ts-substituted complex **4** featured an irreversible oxidation wave at a much higher potential, which could be a result of poor stability of the Cu^{II} product in the presence of weakly coordinating axial NTs groups.
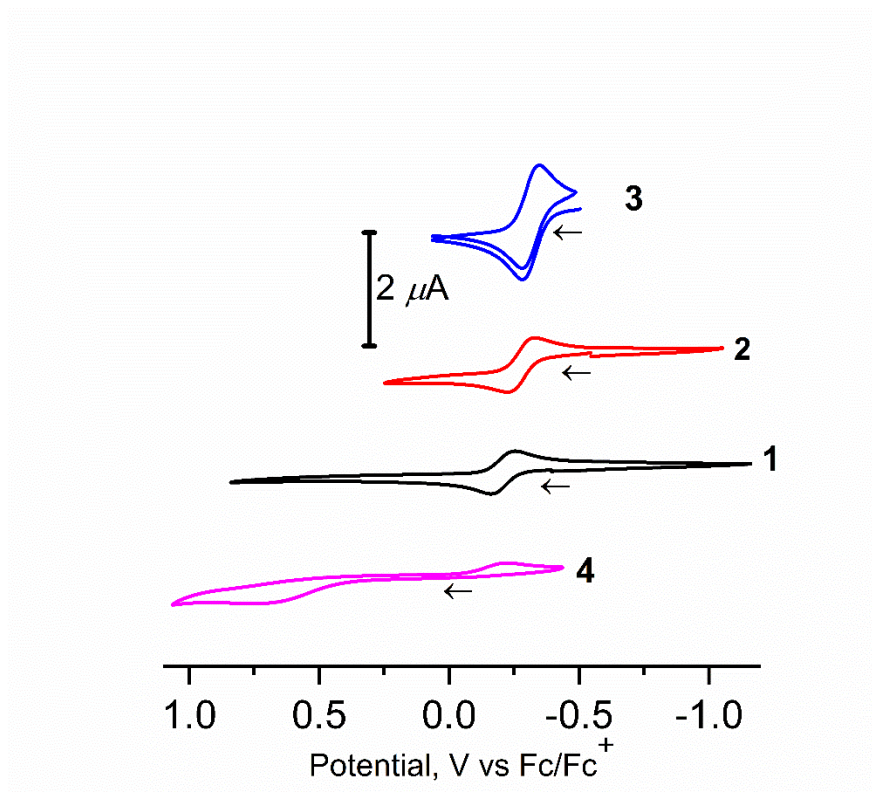
Figure 7. Cyclic voltammograms of complexes **1**, **3**, and **4** (1 mM) in 0.1 M $^nBu_4NPF_6$/MeCN and **2** in 0.1 M $^nBu_4NBF_4$/MeCN solution at 23 °C (scan rate 100 mVs^{-1}; 1.6 mm Pt disk working electrode; the arrow indicates the initial scan direction).

As compared to cationic complexes, electrochemical behavior of neutral copper(I) iodide complexes $^RN4Cu^II$ (**5-10**) is generally more complex and is likely affected by the redox-activity of a free iodide ion that can be released into solution in the presence of an electrolyte, which prevented us from carrying out detailed electrochemical studies on the Cu iodide complex series.[71]

Photophysical properties.

The UV-Vis absorption spectra of complexes $[(^RN4)Cu^I(MeCN)]X$ (**1-4**) in acetonitrile solution and complexes $(^RN4)Cu^II$ (**5-10**) in dichloromethane were recorded (Figure 8). All complexes feature an intense absorption band at 230-300 nm assigned as the ligand-centered transition.

Similarly, free pyridinophane ligands also show an absorption band in this region.[60] ^{R}N4-supported complexes **1-3** and **5-9** where R = H, Me, ^{i}Bu, ^{sec}Bu, ^{neo}Pent, ^{i}Pr are also characterized by a less intense MLCT band ($\varepsilon \approx 10^4$ M^{-1} cm^{-1}) at 390-430 nm (Table 9). By contrast to complexes with alkyl-substituted pyridinophane ligands, the Ts-substituted analogs [(^{Ts}N4)Cu^{I}(MeCN)]PF$_6$ (**4**) and (^{Ts}N4)Cu^{I}I (**10**) did not exhibit any absorption bands above 300 nm.
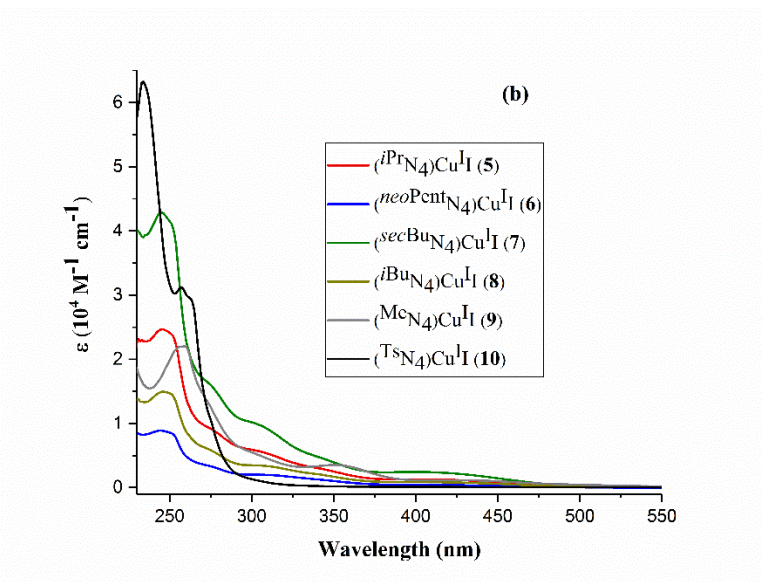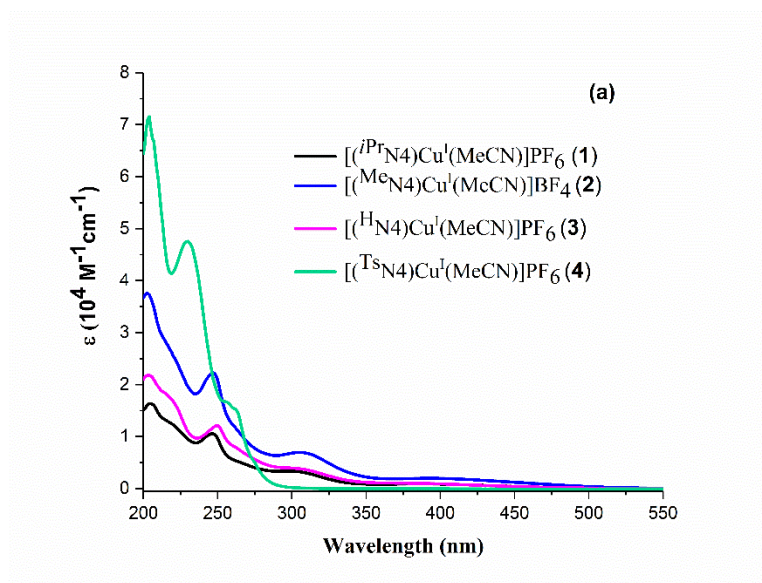
Figure 8. UV-Vis absorbance spectra for complexes [(^{R}N4)Cu^I(MeCN)]X (**1-4**) in acetonitrile (a) and (^{R}N4)Cu^{I}I (**5-10**) in dichloromethane (b).

The emission properties of the cationic and neutral complexes were then studied in the solid state and in solution to elucidate interplay between ligand steric properties and photophysical properties of Cu^I complexes in a series of containing ^{t}Bu, ^{i}Pr, ^{neo}Pent, ^{sec}Bu, ^{i}Bu and Me substituents at the amine. While the cationic acetonitrile complexes [(^{R}N4)Cu^I(MeCN)]X (**1-4**) showed negligible emission in the solid state upon excitation at 400 nm (typically <5%), the neutral copper(I) iodide complexes (^{R}N4)Cu^{I}I **5-9** bearing alkyl substituents at the amine donors exhibited a broad emission band with the maximum in the range of 540-589 nm at 298 K, indicative of the charge-transfer character of the emissive excited states[49, 54, 57, 87] and consistent with previously reported TD-DFT studies (Figure 9).[60] The photophysical properties of complexes (^{R}N4)Cu^{I}I **5-9** as well as comparison with the previously reported complex (^{tBu}N4)Cu^{I}I (**A**) at room temperature are summarized in Table 8. In all cases, the average emission lifetimes were in the microsecond range, varying from 6.3 to 20.02 μs, indicating phosphorescense from the triplet excited state (Figure 10), although TADF cannot be completely excluded.[60, 88] Complex (^{Me}N4)Cu^{I}I (**9**) showed only negligible emission (< 3%) under the same conditions. The emission decay profile could be fit with a mono-exponential curve, except for complex (^{Me}N4)Cu^{I}I (**9**), in which a bi-exponential fit gave two components with lifetimes of 1.70 and 8.39 μs, with an intensity weighted average value of 6.31 μs.
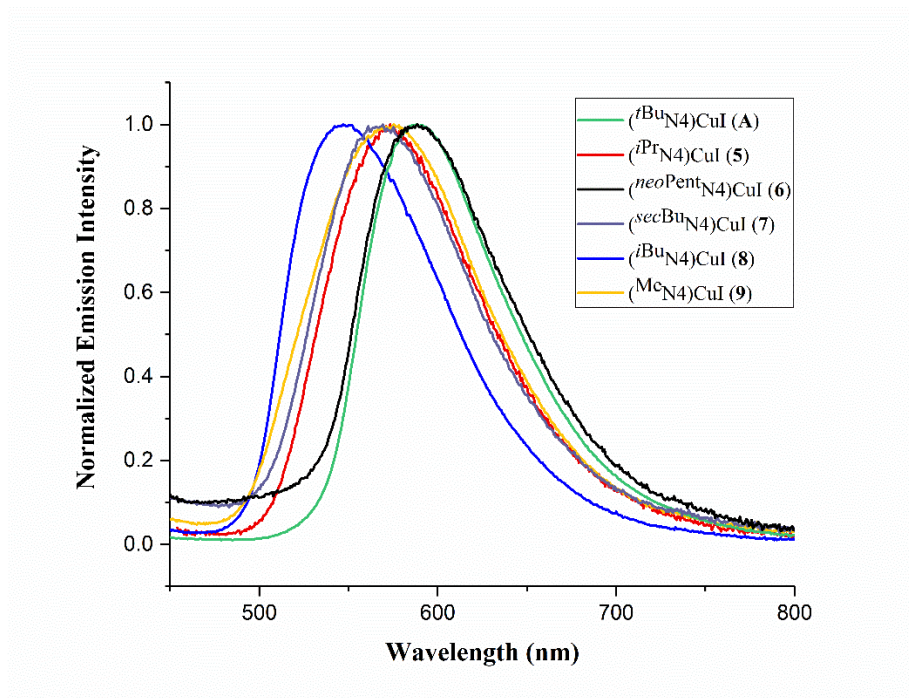
Figure 9. Normalized emission spectra of complexes $^{t\text{Bu}}$N4Cu$^{\text{I}}$I (**A**), $^{i\text{Pr}}$N4Cu$^{\text{I}}$I (**5**), $^{neo\text{Pent}}$N4Cu$^{\text{I}}$I (**6**), $^{sec\text{Bu}}$N4Cu$^{\text{I}}$I (**7**), $^{i\text{Bu}}$N4Cu$^{\text{I}}$I (**8**) and $^{\text{Me}}$N4Cu$^{\text{I}}$I (**9**) in the solid state at 298 K; excitation at 400 nm.
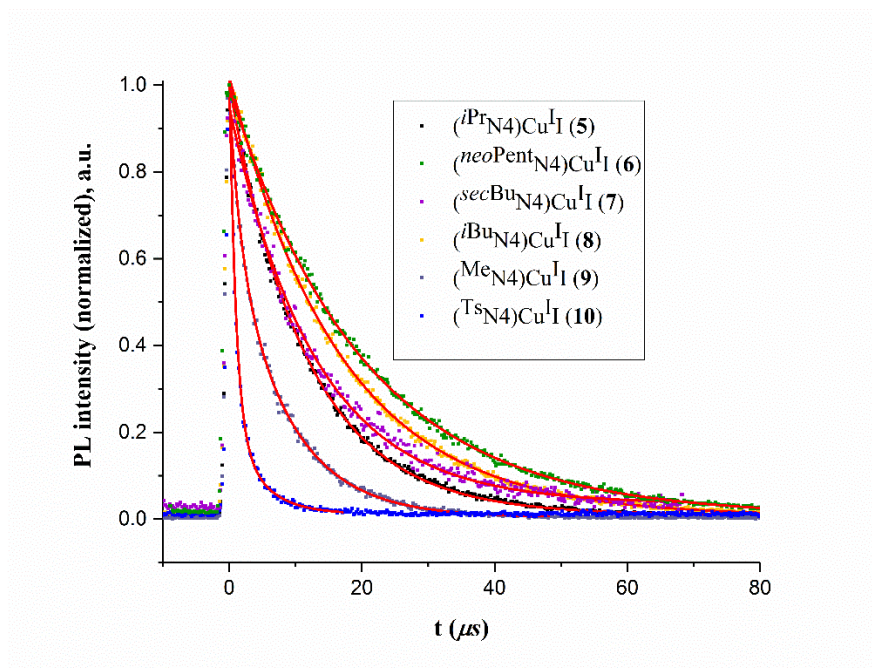
Figure 10. Normalized photoluminescence decay profiles for complexes **5-10** (500-800 nm range) in the solid state at 298 K. Excitation at 400 nm.

Table 8. Photophysical properties of complexes (^{R}N4)Cu^{I}I **5-9** and (^{tBu}N4)Cu^{I}I **A** in the solid state at 298 K.[a]

Complex	λ_{emi} (nm)[b]	Φ[c]	τ (μs)[d]	$k_r \cdot 10^{-4}$ (s^{-1})[e]	$k_{nr} \cdot 10^{-4}$ (s^{-1})[f]	CIE color coordinates (x,y)[g]
(^{tBu}N4)Cu^{I}I (**A**)[h]	585	0.78	15.79	4.94	1.39	0.514, 0.476
(^{iPr}N4)Cu^{I}I (**5**)	576	0.58	11.66	4.97	3.59	0.487, 0.506
(^{neoPent}N4)Cu^{I}I (**6**)	589	0.55	20.02	2.75	2.25	0.549, 0.439
(^{secBu}N4)Cu^{I}I (**7**)	570	0.40	12.96	3.10	4.65	0.323, 0.268
(^{iBu}N4)Cu^{I}I (**8**)	546	0.39	16.69	2.34	3.66	0.414, 0.562
(^{Me}N4)Cu^{I}I (**9**)	570	0.02	6.31[i]	0.32	15.68	0.470, 0.512

[a]All measurements are performed with excitation at 400 nm. [b]Emission maximum. [c]Photoluminescence quantum yields at 298 K (excitation 400 nm). [d]Emission lifetime at 298 K. [e]Radiative decay rate constants were estimated as Φ/τ. [f]Non-radiative decay rate constants calculated as $k_r(1-\Phi)/\Phi$. [g]CIE 1931 chromaticity diagram coordinates. [h]From Ref [60]. [i]Intensity weighted average value based on biexponential fit (calculated from $\alpha_1\tau_1 + \alpha_2\tau_2/(\alpha_1 + \alpha_2)$; where τ_1 = 1.70 and τ_2 = 8.39 are decay components and $\alpha_1 = (A_1/A_1+A_2)$ and $\alpha_2 = (A_2/A_1+A_2)$ are respective amplitudes where A_1 = 0.301 and A_2 = 0.668 are respective contributions)

The comparison of PLQY in Table 8 shows that the highest PLQY was observed for most bulky ^{t}Bu-substituted complex **A**, while the least sterically hindered complex (^{Me}N4)Cu^{I}I (**9**) showed lowest PLQY. Accordingly, the non-radiative decay rate constant k_{nr} was lowest for complex **A** ($1.39 \cdot 10^4$ s^{-1}) and highest for complex **9** ($15.68 \cdot 10^4$ s^{-1}) in this series. Complexes with intermediate steric hindrance at the axial amines, **5-8**, exhibit PLQY in the range of 0.39-0.55 with k_{nr} falling in the intermediate range (($2.25\text{-}4.65)\cdot 10^4$ s^{-1}).

To exclude effects of crystal packing and aggregation on the photophysical properties, we examined the emission properties in solution at 298 K and in frozen solution at 77 K. To our

satisfaction, solutions of complexes bearing $^{i\mathrm{Pr}}$N4 (**5**), $^{neo\mathrm{Pent}}$N4 (**6**), $^{sec\mathrm{Bu}}$N4 (**7**) and $^{i\mathrm{Bu}}$N4 (**8**) in CH$_2$Cl$_2$ at 298 K showed emission at 600-615 nm (Figure 11), and only the complex with the least bulky Me group ($^{\mathrm{Me}}$N4)Cu$^{\mathrm{I}}$I (**9**) showed negligible emission with PLQY < 0.01. In polar coordinating solvents such as alcohols or nitriles, the emission was negligible, while low solubility prevented measurements in benzene and toluene solutions. The comparison of CH$_2$Cl$_2$ solution PLQY data for ($^{\mathrm{R}}$N4)Cu$^{\mathrm{I}}$I **5-9** and ($^{t\mathrm{Bu}}$N4)Cu$^{\mathrm{I}}$I (**A**) shows that PLQY gradually decreases in the order: ^{t}Bu > ^{i}Pr $\approx$ ^{sec}Bu > ^{i}Bu > ^{neo}Pent > Me (Table 9), thus showing clear correlation with the steric bulk. [89-92]
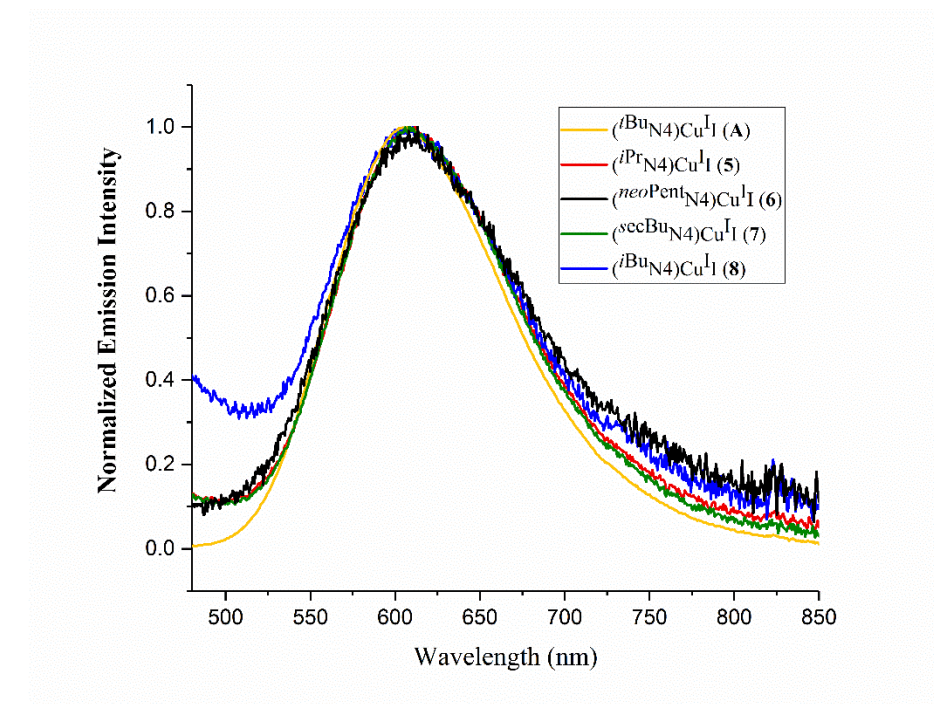
Figure 11. Normalized emission spectra of complexes $^{t\mathrm{Bu}}$N4Cu$^{\mathrm{I}}$I (**A**), $^{i\mathrm{Pr}}$N4Cu$^{\mathrm{I}}$I (**5**), $^{neo\mathrm{Pent}}$N4Cu$^{\mathrm{I}}$I (**6**), $^{sec\mathrm{Bu}}$N4Cu$^{\mathrm{I}}$I (**7**) and $^{i\mathrm{Bu}}$N4Cu$^{\mathrm{I}}$I (**8**) in CH$_2$Cl$_2$ solution at 298 K; excitation at 400 nm.
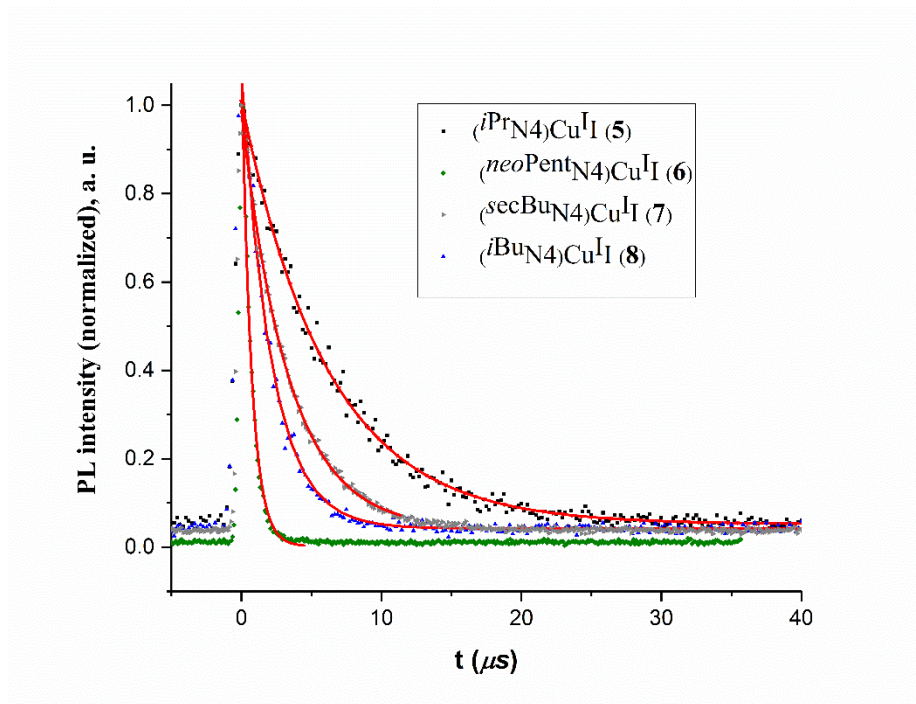
Figure 12. Normalized Photoluminescence decay profiles for CuI complexes **5**-**8** (500-800 nm range) in CH$_2$Cl$_2$ solution at 298 K. Excitation at 400 nm.
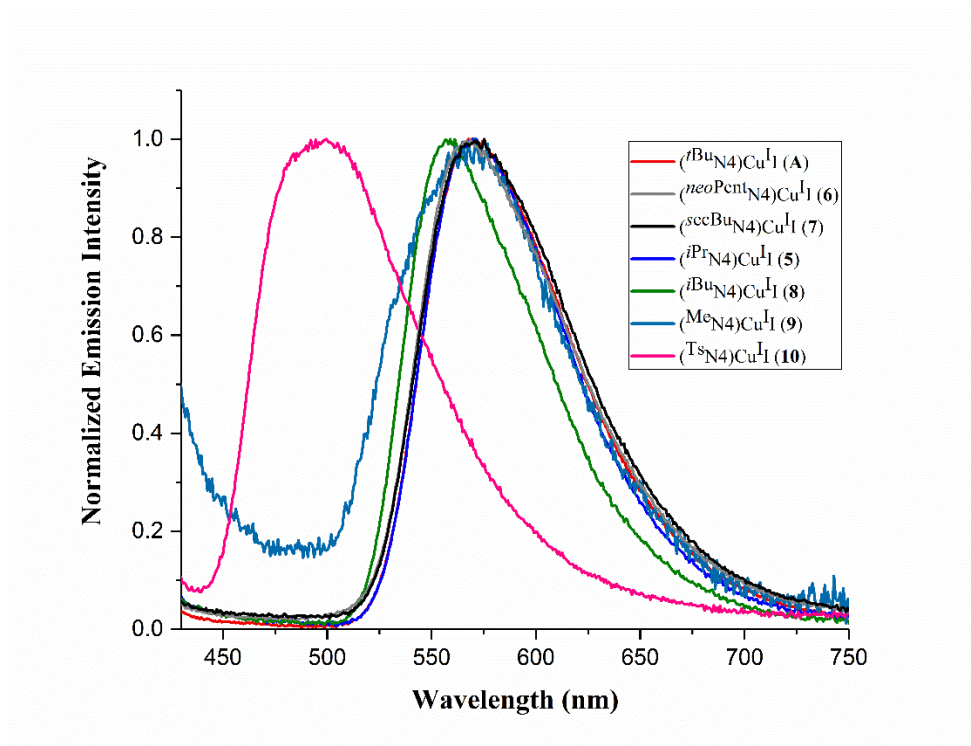
Figure 13. Normalized emission spectra of complexes ^{tBu}N4Cu^I (**A**), ^{iPr}N4Cu^I (**5**), ^{neoPent}N4Cu^I (**6**), ^{secBu}N4Cu^I (**7**), ^{iBu}N4Cu^I (**8**), ^{Me}N4Cu^I (**9**) and ^{Ts}N4Cu^I (**10**) in frozen MeTHF at 77 K; excitation at 400 nm.

Table 9. Photophysical properties of complexes (^{R}N4)Cu^I **5-10** and (^{tBu}N4)Cu^I (**A**) in solution.[a]

Complex	λ_{abs} (nm)[b] [ϵ, (M^{-1}cm^{-1})[c]]	298 K[d] λ_{emi} (nm)[e]	298 K[d] Φ[f]	77 K[g] λ_{emi} (nm)[e]	77 K[g] Φ[f]	τ (μs)[h]	$k_r \cdot 10^{-4}$ (s^{-1})[i]	$k_{nr} \cdot 10^{-5}$ (s^{-1})[j]	CIE color coordinates (x,y)[k]
(^{tBu}N4)Cu^I (**A**)[l]	419 [2031]	600	0.28	568	0.81	4.3	6.51	1.67	0.372, 0.245
(^{iPr}N4)Cu^I (**5**)	415 [1190]	612	0.095	572	0.79	6.17	1.54	1.47	0.388, 0.252
(^{neoPent}N4)Cu^I (**6**)	434 [345]	613	0.025	567	0.91	0.70	3.57	13.9	0.377, 0.242
(^{secBu}N4)Cu^I (**7**)	407 [2380]	609	0.11	575	0.72	3.34	3.29	2.66	0.389, 0.258
(^{iBu}N4)Cu^I (**8**)	417 [811]	610	0.059	559	0.79	2.16	2.73	4.35	0.261, 0.126
(^{Me}N4)Cu^I (**9**)	432 [1090]	n.d.	<0.01	571	0.25	n.d.	n.d.	n.d.	n.d.
(^{Ts}N4)Cu^I (**10**)	n.d.	n.d.	<0.01	499	0.53	n.d.	n.d.	n.d.	n.d.

[a]All measurements are performed with excitation at 400 nm; n.d. – not determined. [b]Absorption maximum. [c]Extinction coefficient. [d]In degassed dichloromethane at 298 K. [e]Emission maximum. [f]Photoluminescence quantum yield. [g]In 2-methyl tetrahydrofuran at 77 K. [h]Emission lifetime at 298 K in CH$_2$Cl$_2$. [i]Radiative decay rate constants were estimated as Φ/τ; measured at 298 K in CH$_2$Cl$_2$. [j]Non-radiative decay rate constants calculated as $k_r(1-\Phi)/\Phi$; measured at 298 K in CH$_2$Cl$_2$. [k]CIE 1931 chromaticity diagram coordinates determined for emission spectrum at 298 K in CH$_2$Cl$_2$. [l]From Ref [60].

As compared to the solid state, the emission lifetimes at 298 K are significantly shorter, falling to a 0.7-6 μs range (Figure 12). While the radiative rate constants remain in a similar range as in the solid state, the solution state k_{nr} increases by about an order of magnitude, indicative of faster non-radiative decay pathways in the solutions of conformationally flexible complexes (^{R}N4)Cu^I. Complex (^{Ts}N4)Cu^I (**10**) showed only negligible emission in the solid state (PLQY < 0.01) and was not emissive in solution, which could be attributed either to its high fluxionality in solution (*vide infra*) as well as a different electronic structure consistent with the lack of MLCT bands at *ca.* 400 nm region; the variation of the excitation source wavelength to higher energies also did

not result in any observable emission. In particular, conformation of the ^{Ts}N4 ligand in complex (^{Ts}N4)Cu^{I}I in solution can differ from other alkyl-substituted complexes, although solution NMR studies did not allow to unambiguously confirm conformational assignment due to high fluxionality of this complex (*vide supra*).

The frozen MeTHF solutions of complexes **A** and **5-10** at 77 K show dramatic increase of PLQY compared to RT measurements reaching 0.79-0.91 for complexes (^{R}N4)Cu^{I}I (R = ^{t}Bu, ^{i}Pr, ^{neo}Pent, ^{sec}Bu and ^{i}Bu) and 0.25 for (^{Me}N4)Cu^{I}I that was non-emissive at RT (Figure 13). This resembles the behavior of 2,9-disubstituted *bis*-phenanthroline Cu^I complexes with long alkyl chain substituents in frozen solutions, which was attributed to the ability of long alkyl chains to prevent significant distortions of the ground and excited states in rigid matrix.[93]

The observed correlation between steric bulk of the amine donor and the photoluminescence quantum yield could be affected by the two main factors. First, as shown by the NMR studies, the steric bulk of the alkyl group affected the rate of the conformational exchange processes in solutions of (^{R}N4)Cu^{I}I (including degenerative exchange), with slower conformational exchange observed for the complexes bearing the more bulky alkyl groups at the amines (vide supra). Second, the steric bulk of the alkyl group also affected the relative stabilities of two different isomers in solution, with tetracoordinate (κ^3-^{R}N4)Cu^{I}I species being more favorable for more sterically demanding R groups. However, in the case of complexes (^{tBu}N4)Cu^{I}I (**A**), (^{neoPent}N4)Cu^{I}I (**6**) and (^{iBu}N4)Cu^{I}I (**8**), only one conformer, (κ^3-^{R}N4)Cu^{I}I, was present in solution in both cases, while solution quantum yield decreased drastically for less bulky and more fluxional complexes **6** and **8** compared to *tert*-butyl-substituted complex **A**, showing that the fluxionality may be the predominant factor affecting solution PLQY.

Similarly, the effect of the ligand steric bulk on the photophysical properties was described for a series of Cu^I complexes with phenanthroline-based ligands, $Cu(NN)_2^+$ and $Cu(NN)(PP)$ ($NN =$ substituted phenanthroline; $PP =$ diphosphine). Introducing bulky substituents at the phenanthroline backbone lead to a significant increase in emission lifetime and PLQY. The detailed investigations of these systems showed that such a strong effect of the ligand steric properties arises due to suppression of the flattening distortion in the CT state, thus preventing non-radiative structural relaxation.[30, 37, 51, 56, 94-96] Although the geometrical changes involved in non-radiative relaxation may differ, suppression of the ligand dynamics achieved by introducing bulky substituents at the weakly interacting amine donors in (^{R}N4)Cu^II complexes is also the main factor that determines PLQY in this series. Although the ligand dynamic process observed by NMR involving degenerative exchange between two axial amines is much slower than non-radiative decay, introduction of the steric bulk at amine substituents might affect fluxionality of the ligand in the excited state in a similar manner. In addition, dynamic processes in the excited state might feature faster rate constants due to charge build-up at the Cu center and at the pyridinophane ligand. [60]

In addition, it has been reported that in the case of tetracoordinate complex $[Cu^I(dmp)_2]^+$ ($dmp =$ 2,9-dimethyl-1,10-phenanthroline), coordination of the Lewis basic solvent such as acetonitrile to the MLCT excited state leads to the "exciplex" quenching.[38,51, 64, 65] In the present (^{R}N4)Cu^I system, the free axial amine moiety can coordinate to the Cu center in the absence of coordinating solvents. Thus, the suppression of the nucleophilic attack by the pendant amine donor to the copper center in the excited state due to presence of bulky alkyl substituents could be another mechanism responsible for higher PLQY observed for complexes with bulky substituents at the amine donors. A higher propensity of complexes with less bulky substituents

to undergo pendant amine donor coordination is observed in the solution behavior of $(^{R}N4)Cu^{I}$ studied by NMR, which shows that only $(^{Me}N4)Cu^{I}$ (**7**) exhibits a substantial fraction of a pentacoordinate $[(\kappa^{4}\text{-}^{R}N4)Cu^{I}]$, and the isomer interconversion is faster as compared to ^{t}Bu and ^{i}Pr-substituted analogs. Moreover, the trend in the oxidation potentials of pentacoordinate complexes **1**-**4** also confirms that stabilization of a Cu^{II} center is favored by less bulky amine donors due to more efficient coordination of the axial amines (*vide supra*).

Interestingly, PLQY in frozen solutions for ^{t}Bu, ^{i}Pr, $^{neo}Pent$, ^{sec}Bu and ^{i}Bu-substituted complexes is very similar, 0.72-0.91, while the Me-substituted complex $(^{Me}N4)Cu^{I}$ (**7**) shows a lower PLQY of 0.25. Similarly, Armaroli, Barigelletti and co-workers reported high emission intensity in frozen solution 2,9-disubstituted *bis*-phenanthroline Cu^{I} complexes with long alkyl chain substituents. [93] At the same time, the Me-substituted *bis*-phenanthroline Cu^{I} complex remained a weak emitter in frozen solution and it was proposed that smaller Me substituents do not prevent excited state distortions even in rigid matrix. By analogy, one could propose that at 77 K, conformational exchange and nucleophilic attack by pendant amine are essentially "frozen" and therefore no significant differentiation of PLQY is observed for complexes $(^{R}N4)Cu^{I}$ (R = ^{t}Bu, ^{i}Pr, $^{neo}Pent$, ^{sec}Bu and ^{i}Bu) all containing bulky alkyl groups that can effectively prevent distortions in the excited state leading to levelling off PLQY to similarly high values of 0.72-0.91. Interestingly, even Ts-substituted complex $(^{Ts}N4)Cu^{I}$ (**10**) which was highly fluxional in solution at RT becomes emissive in frozen solution with PLQY of 0.53, which further confirms the importance of "freezing" conformational lability for emissive properties.

Overall, although Cu-N$_{amine}$ distances are significantly longer than Cu-N$_{pyridine}$ distances, the emissive properties of $(^{R}N4)Cu^{I}$ **5**-**9** complexes are very sensitive to steric requirements of the axial amine arms, which determine dynamic properties of the macrocyclic pyridinophane ligand.

Such sensitivity to the subtle changes at the axial amine environment and its effect on ligand fluxionality are likely the key features that enabled the use of analogous, covalently copolymerized complexes as emissive probes for detecting stress in polymer films.

CONCLUSION

In summary, we have explored in detail the structure, ligand conformational behavior, redox, and photophysical properties of a series of copper(I) complexes with a conformationally fluxional $^RN4$ pyridinophane ligand. Steric requirements of the axial amine substituents in these complexes were shown to play a key role in determining solution behavior and emissive properties of these complexes. The solution NMR studies revealed two types of exchange processes that exist in solutions of ($^RN4$)Cu^{I}I, one involving degenerative exchange between two axial amino groups in a κ^3-coordinated ligand, and another being the exchange between the κ^3- and κ^4-bound ligand isomers. The dynamics of exchange were directly correlated to the steric bulk of the alkyl group at the amines, with complexes containing more bulky alkyl groups at the amines showing slower conformational exchange.

Moreover, we have shown that the mononuclear complexes supported by an N-donor macrocyclic ligand, ($^RN4$)Cu^{I}I, show emissive properties in solution and in the solid state, with the photoluminescence quantum yield that is highly sensitive to the steric bulk of the amine substituents, likely through suppression of the non-radiative decay pathways in less fluxional complexes bearing bulkier alkyl groups. Since the steric bulk of the alkyl group at the amine can be easily controlled by simple synthetic modifications, this offers a convenient strategy for the control of photophysical properties of simple, solution-stable mononuclear Cu^I complexes. Importantly, the current study showed that although increasing steric bulk effects the axial amine-Cu^I center distance, it does not have a negative effect in increasing exchange equilibria

and quantum yield and emission lifetime only improve in the series of simple alkyl substituted complexes studied here. These photophysical properties are adversely affected when substituting an alkyl group for an electron withdrawing Ts moiety. These finding have a direct implication in the design of future dynamic polymer probes,[66] where we will seek to introduce even bulkier, alkyl based substituents in order to decrease the amount of organometallic co-monomer required for visual observation of mechanical stress.

ASSOCIATED CONTENT

Supporting Information.

The following files are available free of charge at http://pubs.acs.org.

Synthesis, characterization, and full NMR, UV-vis and FT-IR spectra of complexes **1-10** (PDF)

X-ray crystallographic data (CIF)

AUTHOR INFORMATION

Corresponding Author

*E-mail: juliak@oist.jp.

Notes

ABBREVIATIONS

^{t}Bu, *tert*-butyl; ^{i}Pr, *iso*-propyl; ^{neo}Pent, *neo*-pentyl; ^{sec}Bu, *sec*-butyl; ^{i}Bu, *iso*-butyl; Me, methyl; CV, cyclic voltammetry; PL, photoluminescence; PLQY; photoluminescence quantum yield; NMR, nuclear magnetic resonance; EXSY, exchange spectroscopy; SST, spin saturation transfers; VT, variable temperature; XRD, X-ray diffraction.

REFERENCES

1.   Chang-Yen, D. A.; Lvov, Y.; McShane, M. J.; Gale, B. K. Electrostatic Self-Assembly of a Ruthenium-Based Oxygen Sensitive Dye Using Polyion–Dye Interpolyelectrolyte Formation. *Sens. Actuators., B: Chem* **2002**, *87*, 336-345.

2.   Cooke, M. W.; Hanan, G. S. Luminescent Polynuclear Assemblies. *Chem. Soc. Rev.* **2007**, *36*, 1466-1476.

3.   Du, P.; Schneider, J.; Brennessel, W. W.; Eisenberg, R. Synthesis and Structural Characterization of a New Vapochromic Pt(II) Complex Based on the 1-Terpyridyl-2,3,4,5,6-Pentaphenylbenzene (Tpppb) Ligand. *Inorg. Chem.* **2008**, *47*, 69-77.

4.   Gong, X.; Robinson, M. R.; Ostrowski, J. C.; Moses, D.; Bazan, G. C.; Heeger, A. J. High-Efficiency Polymer-Based Electrophosphorescent Devices. *Adv. Mater.* **2002**, *14*, 581-585.

5.   Islam, A.; Sugihara, H.; Arakawa, H. Molecular Design of Ruthenium(II) Polypyridyl Photosensitizers for Efficient Nanocrystalline TiO_2 Solar Cells. *J. Photochem. Photobio, A: Chem* **2003**, *158*, 131-138.

6.   Kalyanasundaram, K.; Grätzel, M. Applications of Functionalized Transition Metal Complexes in Photonic and Optoelectronic Devices. *Coord. Chem. Rev.* **1998**, *177*, 347-414.

7.   Keefe, M. H.; Benkstein, K. D.; Hupp, J. T. Luminescent Sensor Molecules Based on Coordinated Metals: A Review of Recent Developments. *Coord. Chem. Rev.* **2000**, *205*, 201-228.

8.   Köhler, A.; Wilson, J. S.; Friend, R. H. Fluorescence and Phosphorescence in Organic Materials. *Adv. Mater.* **2002**, *14*, 701-707.

9.   Mukherjee, S.; Thilagar, P. Recent Advances in Purely Organic Phosphorescent Materials. *Chem. Commun.* **2015**, *51*, 10988-11003.

10.   Muller, G. Luminescent Chiral Lanthanide(III) Complexes as Potential Molecular Probes. *Dalton Trans.* **2009**, 9692-9707.

11.   Ohara, H.; Ogawa, T.; Yoshida, M.; Kobayashi, A.; Kato, M. Reversible Luminescent Colour Changes of Mononuclear Copper(I) Complexes Based on Ligand Exchange Reactions by N-Heteroaromatic Vapours. *Dalton Trans.* **2017**, *46*, 3755-3760.

12.   Ramdass, A.; Sathish, V.; Velayudham, M.; Thanasekaran, P.; Umapathy, S.; Rajagopal, S. Luminescent Sensor for Copper(II) Ion Based on Imine Functionalized Monometallic Rhenium(I) Complexes. *Sens. Actuators., B: Chem* **2017**, *240*, 1216-1225.

13.   Sakaki, S.; Kuroki, T.; Hamada, T. Synthesis of a New Copper(I) Complex, [Cu(Tmdcbpy)$_2$]$^+$ (Tmdcbpy = 4,4′,6,6′-Tetramethyl-2,2′-Bipyridine-5,5′-Dicarboxylic Acid), and Its Application to Solar Cells. *J. Chem. Soc., Dalton Trans.* **2002**, 840-842.

14.   Wei, W.; Wu, M.; Gao, Q.; Zhang, Q.; Huang, Y.; Jiang, F.; Hong, M. A Novel Supramolecular Tetrahedron Assembled from Tetranuclear Copper(I) Cluster Molecules Via Aryl Embrace Interactions. *Inorg. Chem.* **2009**, *48*, 420-422.

15.   Xiang, H.; Cheng, J.; Ma, X.; Zhou, X.; Chruma, J. J. Near-Infrared Phosphorescence: Materials and Applications. *Chem. Soc. Rev.* **2013**, *42*, 6128-6185.

16.   Yook, K. S.; Lee, J. Y. Organic Materials for Deep Blue Phosphorescent Organic Light-Emitting Diodes. *Adv. Mater.* **2012**, *24*, 3169-3190.

17.   Zhang, Q.; Zhou, Q.; Cheng, Y.; Wang, L.; Ma, D.; Jing, X.; Wang, F. Highly Efficient Green Phosphorescent Organic Light-Emitting Diodes Based on CuI Complexes. *Adv. Mater.* **2004**, *16*, 432-436.

18.   Che, C. M.; Kwok, C. C.; Lai, S. W.; Rausch, A. F.; Finkenzeller, W. J.; Zhu, N.; Yersin, H. Photophysical Properties and OLED Applications of Phosphorescent Platinum(II) Schiff Base Complexes. *Chem. Eur. J.* **2010**, *16*, 233-247.

19.   Del Guerzo, A.; Leroy, S.; Fages, F.; Schmehl, R. H. Photophysics of Re(I) and Ru(II) Diimine Complexes Covalently Linked to Pyrene: Contributions from Intra-Ligand Charge Transfer States. *Inorg. Chem.* **2002**, *41*, 359-366.

20.   Fleetham, T.; Li, G.; Li, J. Phosphorescent Pt(II) and Pd(II) Complexes for Efficient, High-Color-Quality, and Stable OLEDs. *Adv. Mater.* **2017**, *29*, 1601861-1601876.

21.   He, L.; Qiao, J.; Duan, L.; Dong, G.; Zhang, D.; Wang, L.; Qiu, Y. Toward Highly Efficient Solid-State White Light-Emitting Electrochemical Cells: Blue-Green to Red Emitting Cationic Iridium Complexes with Imidazole-Type Ancillary Ligands. *Adv. Funct. Mater.* **2009**, *19*, 2950-2960.

22.   Lowry, M. S.; Bernhard, S. Synthetically Tailored Excited States: Phosphorescent, Cyclometalated Iridium(III) Complexes and Their Applications. *Chem. Eur. J.* **2006**, *12*, 7970-7977.

23.   Rausch, A. F.; Murphy, L.; Williams, J. A.; Yersin, H. Improving the Performance of Pt(II) Complexes for Blue Light Emission by Enhancing the Molecular Rigidity. *Inorg. Chem.* **2012**, *51*, 312-319.

24.   Tsuzuki, T.; Tokito, S. Highly Efficient and Low-Voltage Phosphorescent Organic Light-Emitting Diodes Using an Iridium Complex as the Host Material. *Adv. Mater.* **2007**, *19*, 276-280.

25.   Tung, Y. L.; Lee, S. W.; Chi, Y.; Chen, L. S.; Shu, C. F.; Wu, F. I.; Carty, A. J.; Chou, P. T.; Peng, S. M.; Lee, G. H. Organic Light-Emitting Diodes Based on Charge-Neutral Ru[II] Phosphorescent Emitters. *Adv. Mater.* **2005**, *17*, 1059-1064.

26.   Ulbricht, C.; Beyer, B.; Friebe, C.; Winter, A.; Schubert, U. S. Recent Developments in the Application of Phosphorescent Iridium(III) Complex Systems. *Adv. Mater.* **2009**, *21*, 4418-4441.

27.   Wong, W.-Y.; He, Z.; So, S.-K.; Tong, K.-L.; Lin, Z. A Multifunctional Platinum-Based Triplet Emitter for OLED Applications. *Organometallics* **2005**, *24*, 4079-4082.

28.   Yang, C. H.; Cheng, Y. M.; Chi, Y.; Hsu, C. J.; Fang, F. C.; Wong, K. T.; Chou, P. T.; Chang, C. H.; Tsai, M. H.; Wu, C. C. Blue-Emitting Heteroleptic Iridium(III) Complexes Suitable for High-Efficiency Phosphorescent OLEDs. *Angew. Chem. Int. Ed.* **2007**, *46*, 2418-2421.

29.   Zhang, Y.; Liu, Z.; Yang, K.; Zhang, Y.; Xu, Y.; Li, H.; Wang, C.; Lu, A.; Sun, S. A Ruthenium(II) Complex as Turn-on Cu(II) Luminescent Sensor Based on Oxidative Cyclization Mechanism and Its Application in Vivo. *Sci. Rep.* **2015**, *5*, 8172-8176.

30.   Barbieri, A.; Accorsi, G.; Armaroli, N. Luminescent Complexes Beyond the Platinum Group: The d^{10} Avenue. *Chem. Commun.* **2008**, 2185-2193.

31.   Czerwieniec, R.; Hofbeck, T.; Crespo, O.; Laguna, A.; Concepcion Gimeno, M.; Yersin, H. The Lowest Excited State of Brightly Emitting Gold(I) Triphosphine Complexes. *Inorg. Chem.* **2010**, *49*, 3764-3767.

32.   Ford, P. C.; Cariati, E.; Bourassa, J. Photoluminescence Properties of Multinuclear Copper(I) Compounds. *Chem. Rev.* **1999**, *99*, 3625-3648.

33.   Hsu, C. W.; Lin, C. C.; Chung, M. W.; Chi, Y.; Lee, G. H.; Chou, P. T.; Chang, C. H.; Chen, P. Y. Systematic Investigation of the Metal-Structure-Photophysics Relationship of Emissive d^{10}-Complexes of Group 11 Elements: The Prospect of Application in Organic Light Emitting Devices. *J. Am. Chem. Soc.* **2011**, *133*, 12085-12099.

34.   Liu, Z.; Qiu, J.; Wei, F.; Wang, J.; Liu, X.; Helander, M. G.; Rodney, S.; Wang, Z.; Bian, Z.; Lu, Z.; Thompson, M. E.; Huang, C. Simple and High Efficiency Phosphorescence Organic Light-Emitting Diodes with Codeposited Copper(I) Emitter. *Chem. Mater.* **2014**, *26*, 2368-2373.

35.   Matsumoto, K.; Shindo, T.; Mukasa, N.; Tsukuda, T.; Tsubomura, T. Luminescent Mononuclear Ag(I)-Bis(Diphosphine) Complexes: Correlation between the Photophysics and the Structures of Mononuclear Ag(I)-Bis(Diphosphine) Complexes. *Inorg. Chem.* **2010**, *49*, 805-814.

36.   Wing-Wah Yam, V.; Kam-Wing Lo, K. Luminescent Polynuclear d[10] Metal Complexes. *Chem. Soc. Rev.* **1999**, *28*, 323-334.

37.   Lavie-Cambot, A. l.; Cantuel, M.; Leydet, Y.; Jonusauskas, G.; Bassani, D. M.; McClenaghan, N. D. Improving the Photophysical Properties of Copper(I) Bis(Phenanthroline) Complexes. *Coord. Chem. Rev.* **2008**, *252*, 2572-2584.

38.   Armaroli, N.; Accorsi, G.; Cardinali, F.; Listorti, A. In *Photochemistry and Photophysics of Coordination Compounds I*; Springer Berlin Heidelberg: Berlin, Heidelberg, 2007; Vol. 280.

39.   Horváth, O. Photochemistry of Copper(I) Complexes. *Coord. Chem. Rev.* **1994**, *135*, 303-324.

40.   Nishikawa, M.; Sano, T.; Washimi, M.; Takao, K.; Tsubomura, T. Emission Properties and Cu(I)-Cu(I) Interaction in 2-Coordinate Dicopper(I)-Bis(N-Heterocyclic)Carbene Complexes. *Dalton Trans.* **2016**, *45*, 12127-12136.

41.   Hofbeck, T.; Monkowius, U.; Yersin, H. Highly Efficient Luminescence of Cu(I) Compounds: Thermally Activated Delayed Fluorescence Combined with Short-Lived Phosphorescence. *J. Am. Chem. Soc.* **2015**, *137*, 399-404.

42.   Nishikawa, M.; Wakita, Y.; Nishi, T.; Miura, T.; Tsubomura, T. Long-Lived and Oxygen-Responsive Photoluminescence in the Solid State of Copper(I) Complexes Bearing Fluorinated Diphosphine and Bipyridine Ligands. *Dalton Trans.* **2015**, *44*, 9170-9181.

43.   Marion, R.; Sguerra, F.; Di Meo, F.; Sauvageot, E.; Lohier, J.-F.; Daniellou, R.; Renaud, J.-L.; Linares, M.; Hamel, M.; Gaillard, S. NHC Copper(I) Complexes Bearing Dipyridylamine Ligands: Synthesis, Structural, and Photoluminescent Studies. *Inorg. Chem.* **2014**, *53*, 9181-9191.

44.   Bizzarri, C.; Strabler, C.; Prock, J.; Trettenbrein, B.; Ruggenthaler, M.; Yang, C.-H.; Polo, F.; Iordache, A.; Brüggeller, P.; Cola, L. D. Luminescent Dinuclear Cu(I) Complexes Containing Rigid Tetraphosphine Ligands. *Inorg. Chem.* **2014**, *53*, 10944-10951.

45.   Krylova, V. A.; Djurovich, P. I.; Aronson, J. W.; Haiges, R.; Whited, M. T.; Thompson, M. E. Structural and Photophysical Studies of Phosphorescent Three-Coordinate Copper(I) Complexes Supported by an N-Heterocyclic Carbene Ligand. *Organometallics* **2012**, *31*, 7983-7993.

46.   Krylova, V. A.; Djurovich, P. I.; Whited, M. T.; Thompson, M. E. Synthesis and Characterization of Phosphorescent Three-Coordinate Cu(I)-NHC Complexes. *Chem. Commun.* **2010**, *46*, 6696-6698.

47.   Lotito, K. J.; Peters, J. C. Efficient Luminescence from Easily Prepared Three-Coordinate Copper(I) Arylamidophosphines. *Chem. Commun.* **2010**, *46*, 3690-3692.

48.   Miller, A. J. M.; Dempsey, J. L.; Peters, J. C. Long-Lived and Efficient Emission from Mononuclear Amidophosphine Complexes of Copper. *Inorg. Chem.* **2007**, *46*, 7244-7246.

49.   Tsuboyama, A.; Kuge, K.; Furugori, M.; Okada, S.; Hoshino, M.; Ueno, K. Photophysical Properties of Highly Luminescent Copper(I) Halide Complexes Chelated with 1,2-Bis(Diphenylphosphino)Benzene. *Inorg. Chem.* **2007**, *46*, 1992-2001.

50.   Harkins, S. B.; Peters, J. C. A Highly Emissive Cu_2N_2 Diamond Core Complex Supported by a [PNP]⁻Ligand. *J. Am. Chem. Soc.* **2005**, *127*, 2030-2031.

51.   McMillin, D. R.; McNett, K. M. Photoprocesses of Copper Complexes That Bind to DNA. *Chem. Rev.* **1998**, *98*, 1201-1220.

52.   Blasse, G.; McMillin, D. R. On the Luminescence of Bis (Triphenylphosphine) Phenanthroline Copper (I). *Chem. Phys. Lett.* **1980**, *70*, 1-3.

53.   Araki, H.; Tsuge, K.; Sasaki, Y.; Ishizaka, S.; Kitamura, N. Luminescence Ranging from Red to Blue: A Series of Copper(I)−Halide Complexes Having Rhombic $\{Cu_2(M-X)_2\}$ (X = Br and I) Units with N-Heteroaromatic Ligands. *Inorg. Chem.* **2005**, *44*, 9667-9675.

54.   Okano, Y.; Ohara, H.; Kobayashi, A.; Yoshida, M.; Kato, M. Systematic Introduction of Aromatic Rings to Diphosphine Ligands for Emission Color Tuning of Dinuclear Copper(I) Iodide Complexes. *Inorg. Chem.* **2016**, *55*, 5227-5236.

55.   Chai, W.; Hong, M.; Song, L.; Jia, G.; Shi, H.; Guo, J.; Shu, K.; Guo, B.; Zhang, Y.; You, W.; Chen, X. Three Reversible Polymorphic Copper(I) Complexes Triggered by Ligand Conformation: Insights into Polymorphic Crystal Habit and Luminescent Properties. *Inorg. Chem.* **2015**, *54*, 4200-4207.

56.   Cunningham, C. T.; Cunningham, K. L. H.; Michalec, J. F.; McMillin, D. R. Cooperative Substituent Effects on the Excited States of Copper Phenanthrolines. *Inorg. Chem.* **1999**, *38*, 4388-4392.

57.   Ohara, H.; Kobayashi, A.; Kato, M. Simple and Extremely Efficient Blue Emitters Based on Mononuclear Cu(I)-Halide Complexes with Delayed Fluorescence. *Dalton Trans.* **2014**, *43*, 17317-17323.

58.   Kaeser, A.; Mohankumar, M.; Mohanraj, J.; Monti, F.; Holler, M.; Cid, J.-J.; Moudam, O.; Nierengarten, I.; Karmazin-Brelot, L.; Duhayon, C.; Delavaux-Nicot, B.; Armaroli, N.;

Nierengarten, J.-F. Heteroleptic Copper(I) Complexes Prepared from Phenanthroline and Bis-Phosphine Ligands. *Inorg. Chem.* **2013**, *52*, 12140-12151.

59.   Ohara, H.; Kobayashi, A.; Kato, M. Effects of N-Heteroaromatic Ligands on Highly Luminescent Mononuclear Copper(I)–Halide Complexes. *C. R. Chim.* **2015**, *18*, 766-775.

60.   Filonenko, G. A.; Fayzullin, R. R.; Khusnutdinova, J. R. Intramolecular Non-Covalent Interactions as a Strategy Towards Controlled Photoluminescence in Copper(I) Complexes. *J. Mater. Chem. C* **2017**, *5*, 1638-1645.

61.   Khusnutdinova, J. R.; Luo, J.; Rath, N. P.; Mirica, L. M. Late First-Row Transition Metal Complexes of a Tetradentate Pyridinophane Ligand: Electronic Properties and Reactivity Implications. *Inorg. Chem.* **2013**, *52*, 3920-3932.

62.   Meneghetti, S. P.; Lutz, P. J.; Kress, J. Neutral and Cationic Palladium(II) Complexes of a Diazapyridinophane. Structure, Fluxionality, and Reactivity toward Ethylene. *Organometallics* **2001**, *20*, 5050-5055.

63.   Khusnutdinova, J. R.; Rath, N. P.; Mirica, L. M. The Conformational Flexibility of the Tetradentate Ligand ^{tBu}N4 is Essential for the Stabilization of (^{tBu}N4)Pd^{III} Complexes. *Inorg. Chem.* **2014**, *53*, 13112-13129.

64.   Chen, L. X.; Shaw, G. B.; Novozhilova, I.; Liu, T.; Jennings, G.; Attenkofer, K.; Meyer, G. J.; Coppens, P. MLCT State Structure and Dynamics of a Copper(I) Diimine Complex Characterized by Pump-Probe X-Ray and Laser Spectroscopies and DFT Calculations. *J. Am. Chem. Soc.* **2003**, *125*, 7022-7034.

65.   Chen, L. X.; Jennings, G.; Liu, T.; Gosztola, D. J.; Hessler, J. P.; Scaltrito, D. V.; Meyer, G. J. Rapid Excited-State Structural Reorganization Captured by Pulsed X-Rays. *J. Am. Chem. Soc.* **2002**, *124*, 10861-10867.

66.   Filonenko, G. A.; Khusnutdinova, J. R. Dynamic Phosphorescent Probe for Facile and Reversible Stress Sensing. *Adv. Mater.* **2017**, *29*, 1700563-1700568.

67.   Tang, F.; Qu, F.; Khusnutdinova, J. R.; Rath, N. P.; Mirica, L. M. Structural and Reactivity Comparison of Analogous Organometallic Pd(III) and Pd(IV) Complexes. *Dalton Trans* **2012**, *41*, 14046-14050.

68.   Bottino, F.; Di Grazia, M.; Finocchiaro, P.; Fronczek, F. R.; Mamo, A.; Pappalardo, S. Reaction of Tosylamide Monosodium Salt with Bis(Halomethyl) Compounds: An Easy Entry to Symmetrical N-Tosyl Aza Macrocycles. *J. Org. Chem.* **1988**, *53*, 3521-3529.

69.   Kubas, G. J.; Monzyk, B.; Crumblis, A. L. In *Inorg. Synth.*; John Wiley & Sons, Inc.: 2007.

70.   Jarek, R. L.; Flesher, R. J.; Shin, S. K. Kinetics of Internal Rotation of N,N-Dimethylacetamide; a Spin-Saturation Transfer Experiment. An Undergraduate Physical Chemistry Experiment Using FT-NMR to Determine an Internal Rotational Barrier. *J. Chem. Educ.* **1997**, *74*, 978-982.

71.   See the Supporting Information.

72.   Farrugia, L. J. Wingx and Ortep for Windows: An Update. *J. Appl. Crystallogr.* **2012**, *45*, 849-854.

73.   Sheldrick, G. ShelXT - Integrated Space-Group and Crystal-Structure Determination. *Acta Crystallogr., Sect. A* **2015**, *71*, 3-8.

74.   Sheldrick, G. Crystal Structure Refinement with ShelXL. *Acta Crystallogr., Sect. C* **2015**, *71*, 3-8.

75.   Flack, H. D.; Bernardinelli, G. Reporting and Evaluating Absolute-Structure and Absolute-Configuration Determinations. *J. Appl. Crystallogr.* **2000**, *33*, 1143-1148.

76.   Kühn, U.; Warzeska, S.; Pritzkow, H.; Krämer, R. A Bioinspired Dicopper(II) Catalyst for the Transesterification of Dimethyl Phosphate. *J. Am. Chem. Soc.* **2001**, *123*, 8125-8126.

77.   Jagoda, M.; Warzeska, S.; Pritzkow, H.; Wadepohl, H.; Imhof, P.; Smith, J. C.; Krämer, R. Catalytic Transesterification of Dialkyl Phosphates by a Bioinspired Dicopper(II) Macrocyclic Complex. *J. Am. Chem. Soc.* **2005**, *127*, 15061-15070.

78.   Warzeska, S.; Kramer, R. A Dicopper (II) Complex of a New Octaaza Macrocycle: A Receptor in the Entatic State. *Chem. Commun.* **1996**, 499-500.

79.   Prince, E. International Tables for Crystallography, 3rd Edition. **2004**, *Volume C, Mathematical, Physical and Chemical Tables*.

80.   Addison, A. W.; Rao, T. N.; Reedijk, J.; van Rijn, J.; Verschoor, G. C. Synthesis, Structure, and Spectroscopic Properties of Copper(II) Compounds Containing Nitrogen-Sulphur Donor Ligands; the Crystal and Molecular Structure of Aqua[1,7-Bis(N-Methylbenzimidazol-2'-yl)-2,6-Dithiaheptane]Copper(II) Perchlorate. *J. Chem. Soc., Dalton Trans.* **1984**, 1349-1356.

81.   Yang, L.; Powell, D. R.; Houser, R. P. Structural Variation in Copper(I) Complexes with Pyridylmethylamide Ligands: Structural Analysis with a New Four-Coordinate Geometry Index, τ_4. *Dalton Trans.* **2007**, 955-964.

82.   Okuniewski, A.; Rosiak, D.; Chojnacki, J.; Becker, B. Coordination Polymers and Molecular Structures among Complexes of Mercury(II) Halides with Selected 1-Benzoylthioureas. *Polyhedron* **2015**, *90*, 47-57.

83.   The crystals were obtained by slow diffusion of diethyl ether vapors into dichloromethane solution; the crystalline product was analyzed by XRD and the structure was submitted to CCDC, 1833073.

84.   All spectra were recorded using 600 MHz NMR spectrometer. Due to larger chemical shift difference between *meta*-protons in other complexes, such comparison cannot be made directly.

85.   Similar treatment was not possible for complex **5** as three-site exchange occurs under these conditions, including degenerative exchange in tetracoordinate complex and formation of a pentacoordinate isomer. For complex **7**, selective signal irradiation could not be achieved due to close spacing between aromatic peaks.

86.   Zanello, P.; Nervi, C.; Fabrizi de Biani, F. *Inorganic Electrochemistry: Theory, Practice and Application, 2nd Edition*. Royal Society of Chemistry: 2012.

87.   Zink, D. M.; Volz, D.; Baumann, T.; Mydlak, M.; Flügge, H.; Friedrichs, J.; Nieger, M.; Bräse, S. Heteroleptic, Dinuclear Copper(I) Complexes for Application in Organic Light-Emitting Diodes. *Chem. Mater.* **2013**, *25*, 4471-4486.

88.   Emission spectra of complexes **A**, **5** and **8** in THF show hypsochromic shift at 77 K as compared to spectra at 298 K which is not consistent with TADF (*e.g.* See Nitsch, J. *et al*. *Chem. Comm*. **2016**, *52*, 2932-2935).

89.   Williford, C. J.; Stevens, E. P. Strain Energies as a Steric Descriptor in Qsar Calculations. *QSAR & Comb. Sci.* **2004**, *23*, 495-505.

90.   Eliel, E. L.; Wilen, S. H.; Mander, L. N. *Stereochemistry of Organic Compounds*. Wiley & Sons: 1994.

91.   Anslyn, E. V.; Dougherty, D. A.; Dougherty, E. V.; University Science, B. *Modern Physical Organic Chemistry*. University Science Books: 2006.

92.   In particular, the correlation is observed with AG_{60} steric parameter based on different stability of *gauche* and *anti* conformers of substituted propanes, described in Ref. 89, and *A* values (see Refs 89-91).

93.   Felder, D.; Nierengarten, J.-F.; Barigelletti, F.; Ventura, B.; Armaroli, N. Highly Luminescent Cu(I)−Phenanthroline Complexes in Rigid Matrix and Temperature Dependence of the Photophysical Properties. *J. Am. Chem. Soc.* **2001**, *123*, 6291-6299.

94.   Cunningham, C. T.; Moore, J. J.; Cunningham, K. L. H.; Fanwick, P. E.; McMillin, D. R. Structural and Photophysical Studies of $Cu(NN)_2^+$ Systems in the Solid State. Emission at Last from Complexes with Simple 1,10-Phenanthroline Ligands. *Inorg. Chem.* **2000**, *39*, 3638-3644.

95.   Cuttell, D. G.; Kuang, S.-M.; Fanwick, P. E.; McMillin, D. R.; Walton, R. A. Simple Cu(I) Complexes with Unprecedented Excited-State Lifetimes. *J. Am. Chem. Soc.* **2002**, *124*, 6-7.

96.   Everly, R. M.; Ziessel, R.; Suffert, J.; McMillin, D. R. Steric Influences on the Photoluminescence from Copper(I) Phenanthrolines in Rigid Media. *Inorg. Chem.* **1991**, *30*, 559-561.

For Table of Contents Only:
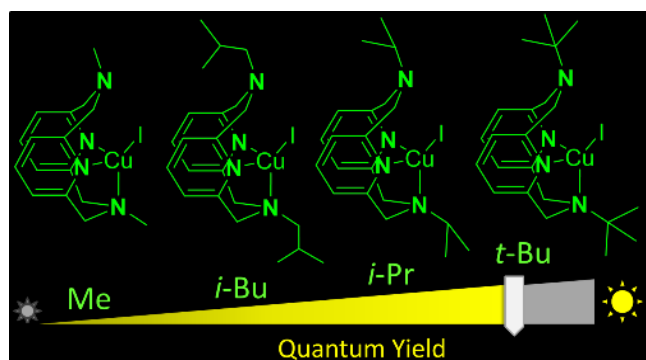
Ligand steric bulk affects dynamic behavior of pyridinophane copper(I) complexes, with more bulky ligands showing slower configurational exchange. Accordingly, correlation is found between steric bulk and photoluminescence quantum yield, with sterically hindered systems showing higher quantum yield in solution and solid state.